Global temperature calibrations based on 3-hydroxy fatty acids in lacustrine settings

Sai Ke [a*], Pierre Sabatier [b], Christelle Anquetil [a], Arnaud Huguet [a*]

a Sorbonne Université, CNRS, EPHE, PSL, UMR METIS, Paris, France
b Université Savoie Mont Blanc, CNRS, UMR EDYTEM, Le Bourget du Lac, France

Abstract

Lakes are important archives of palaeoclimate records on the continent and decoding them could improve the parameterization of climate models to better predict the future. However, the limited temperature proxies currently applicable in lake environments make high-resolution climate records scarce. 3-hydroxy fatty acids (3-OH FAs) are bacterial lipids which have recently been proposed as temperature proxies in terrestrial and aquatic settings, with only regional studies in lakes. Here, the aim was to investigate the applicability of 3-OH FAs as temperature proxies in lakes at the global scale using an extended dataset (n=241) consisting of previously published data (n=113) and 128 newly analyzed lake surface sediments from all over the globe. The distribution of 3-OH FAs in lakes was shown to be generally homogeneous and distinct from the one observed in global soil and marine datasets, suggesting a major contribution of *in situ* production for these lipids at the global scale. Among the lakes, modest changes in 3-OH FA signatures were observed, likely reflecting variations in lipid sources and/or microbial diversity, with general independence of the 3-OH FA signal to climatic forcing, supporting the applicability of these compounds across lakes with diverse geographic settings. Only weak linear relationships between 3-OH FA relative abundances and temperature were observed. Three machine-learning models (multiple linear regression, random forest and TabPFN) were tested and revealed moderate to strong correlations with temperature. The application of the TabPFN model to our global lacustrine dataset especially generated a strong calibration to the mean temperature of Months Above Freezing (MAF), with an R^2 of 0.75 and RMSE of 3.2 °C. The newly developed calibrations were applied to the only 3-OH FA lake core record available to date. The global model based on the TabPFN algorithm provided reliable reconstructions of mean summer temperature. Meanwhile, strong regional effects were found in the models reconstructing mean annual air temperatures and MAF temperatures, leading to the development of local 3-OH FA temperature calibrations based on the same machine-learning algorithms. The latter provided similar trends with 3-OH FA-based (RAN_{13} index) and brGDGT-based (MBT'_{5Me} index) regional records. Altogether, these results demonstrate the potential of 3-OH FAs as temperature proxies in global lakes through the use of refined statistical models.

Keywords: 3-hydroxy fatty acids; lipid biomarkers; palaeoclimate proxies; machine learning

* Corresponding authors. Email addresses: arnaud.huguet@sorbonne-universite.fr (A. Huguet); sai.ke@sorbonne-universite.fr (S. Ke).

1. Introduction

Lake sediment preserves continuous, high-resolution records of past continental climate. Specifically, temperature is among the most fundamental climate parameters and directly affects human activities (Cerri et al., 2007; Lehtonen, 1996), sea level rise (Tebaldi et al., 2021), biodiversity (Malcolm et al., 2006), and the frequency of extreme weather events (Diffenbaugh et al., 2017). Revealing past temperature variations can contribute directly to the parameterization of climate models to predict future scenarios. To date, compared with marine settings, only a limited number of temperature proxies have been developed for lake settings, such as lipid biomarkers (Castañeda and Schouten, 2011), microfossil ecological niches (Lotter et al., 1997), and stable isotopes of biogenic carbonates (Hammarlund et al., 2002). Among these proxies, lipid biomarkers are of particular interest in continental regions because of their ubiquity across a large range of locations. Branched glycerol dialkyl glycerol tetraethers (brGDGTs) have been increasingly popular over the last years as they are to date the only lipid biomarkers which can be used as temperature proxies in both aquatic and terrestrial settings. BrGDGTs are membrane-spanning lipids of bacterial origin. Their exact producers are still unknown, even though some of them belong to the *Acidobacteria* phylum (Sinninghe Damsté et al., 2011; Sinninghe Damsté et al., 2018; Halamka et al., 2023). The bacterial lipid distribution is an efficient indicator of environmental changes, as bacteria are able to modulate membrane lipid composition to maintain suitable membrane fluidity and permeability, a process known as homeoviscous adaptation (Sinensky, 1974). The methylation and cyclisation degree of brGDGTs were shown to vary with temperature and pH, respectively, leading to the development of indices reflecting these distribution changes (Weijers et al., 2007; De Jonge et al., 2014). The MBT'$_{5Me}$ – methylation index of 5-methyl brGDGTs – was especially correlated with temperature in soils and lakes and applied as proxy for temperature reconstructions (De Jonge et al., 2014; Watson et al., 2018; Bittner et al., 2022; Wu et al., 2023; Loomis et al., 2012; Hou et al., 2024). However, large uncertainties persist in global brGDGT temperature models, with root mean square error (RMSE)>4°C in soils and peats (e.g. Véquaud et al., 2022) and > 2°C in lakes (Zhu et al., 2025), as several interconnected factors can affect the distribution of these lipids. First, brGDGTs in lake sediments can have a mixed origin: they can originate from the catchment soils but can also be produced *in situ* in the water column and/or sediments (Tierney and Russell, 2009; Zhao et al., 2021; Van Bree et al., 2020). Second, the diversity of bacterial communities can vary significantly across lakes, which can lead to variations in brGDGT distribution (Liang et al., 2024; Wu et al., 2021). In addition, the reconstructed temperature may be biased to warmer seasons due to preferential seasonal bacterial activity (Deng et al., 2016; De Jonge et al., 2014; Raberg et al., 2021). The lack of knowledge of the exact brGDGT producers prevents a full understanding of the lipid adaptation to environmental changes through culture experiments, which remain scarce (Halamka et al., 2023; Chen et al, 2022). Altogether, these limitations reduce the reliability of brGDGTs as standalone lacustrine temperature

proxies, highlighting the need for independent and complementary proxies to validate and strengthen continental paleoclimate reconstructions.

Recently, a group of lipids named 3-hydroxy fatty acids (3-OH FAs) has been proposed as novel temperature proxies in soils (Huguet et al., 2019; Véquaud et el., 2021; Wang et al., 2016, 2021) and holds the potential to be applied in lake settings (Hou et al., 2026; Ke et al., 2026; Yang et al., 2021). 3-OH FAs with chain lengths spanning 10 to 18 carbon atoms are known to be produced by all species of gram-negative bacteria (GNB), which are also ubiquitously distributed in both soils and lakes, like the brGDGTs. They are classified into three groups on the basis of the presence and position of an additional methyl group: *iso* (methyl group on the penultimate carbon), *anteiso* (methyl group on the antepenultimate carbon), and *normal* (straight chain). Such structural differences can be associated with the physical features of the membrane they form. For example, the branched structure of *anteiso* and *iso* groups corresponds to higher membrane fluidity and is preferred over straight-chain *normal* isomers in cold environments (Poger et al., 2014; Mostofian et al., 2019; Mansilla et al., 2004). Therefore, a theoretical negative correlation of temperature and branched compound abundance will be expected and has been observed in both culture experiments (Hellequin et al., 2023) and environmental sample analyses (Wang et al., 2016; Huguet et al., 2019; Véquaud et al., 2021). Thus, an empirical negative linear correlation between the *anteiso*-to-*normal* ratio of 3-OH FAs with 15 and 17 carbon atoms (RAN_{15} and RAN_{17}, respectively) and Mean Annual Air Temperature (MAAT) has been found in soils from multiple locations, such as China, Tanzania, and Peruvian Andes (Wang et al., 2016 and 2021; Huguet et al., 2019; Véquaud et al., 2021), but remains weak to absent in soils from other regions, such as central Italy, Chilean Andes, and French Alps. The fact that distinct relationships between 3-OH FA distribution and temperature were observed in soils from different sites prevented the development of temperature calibrations based on the aforementioned indices at the global scale. This regional dependency of the 3-OH FA response to temperature was also observed in lakes. Thus, a negative correlation between MAAT and the RAN_{13} index (ratio of *a*-C_{13} to *n*-C_{13} 3-OH FAs) was observed in lakes from China (Yang et al., 2021) and U.S. East Coast (Hou et al., 2026). Such a linear relationship was not observed in lakes from the French Alps (n=52), and Chile (n=20; Ke et al., 2026).

These regional discrepancies could be due to three main reasons. First, non-thermal factors, such as salinity, pH, and oxygen content, could also impact Gram-negative bacteria and their associated membrane lipids, including 3-OH FA distribution (Peter and Sommaruga, 2016; Shang et al., 2022; Weise et al., 2016; Yannarell and Triplett, 2005). Second, as previously observed for brGDGTs (Tierney and Russell, 2009; Zhao et al., 2021; Van Bree et al., 2020), the mixed sources of 3-OH FAs (soil inputs and *in situ* lacustrine production) may complicate the understanding of the lipid signal preserved in sediments. The contribution of *in situ*-produced 3-OH FAs in lakes has been highlighted by all recent studies (Hou et al., 2026; Ke et al., 2026; Wang et al., 2025; Yang et al., 2021), while the extent of a parallel terrestrial influence can be lake-dependent and reflected in the distribution of 3-OH FAs (Ke et

al., 2026). Last, environmental changes cannot only trigger homeoviscous adaptation but also bacterial community shifts (Yannarell and Triplett, 2005; Lindström et al., 2005), a phenomenon called community effect (De Jonge et al., 2019). Different strains of GNB can have distinct 3-OH FA profiles (Baumann et al., 2022), and the resulting variability in lipid distribution could obscure the physiological signals (Zeng et al., 2026). The three aforementioned mechanisms could at least partly explain the distinct linear correlation patterns observed to date between 3-OH FA distribution and temperatures across lakes from different regions (Yang et al., 2021; Hou et al., 2026; Ke et al., 2026). This could limit the applicability of 3-OH FAs as temperature proxies in highly diverse lakes at the global scale using linear models.

Such limitations may be overcome using machine-learning algorithms. The latter have been shown to be powerful tool to analyze complex, multi-variable, and/or non-linear data relationships. Over the last years, they have been widely used to develop global temperature calibrations based on lipid biomarkers, including GDGTs (Pearson et al., 2025; Dearing Crampton-Flood et al., 2020; Dunkley Jones et al., 2020; Häggi et al., 2023; Martínez-Sosa et al., 2021) and 3-OH FAs (Wang et al., 2021; Véquaud et al., 2021; Guria et al., 2026). The models based on machine-learning algorithms integrate the full lipid profiles and focus on the temperature response while taking into account the combined influence of a suite of environmental factors. To date, such algorithms were used to develop global MAAT calibrations based on 3-OH FAs in soil settings (Wang et al., 2021; Véquaud et al., 2021). In lakes, the potential of machine-learning models to build lacustrine temperature calibrations based on 3-OH FAs was recently demonstrated by Ke et al. (2026). Nevertheless, the associated models were built from a small lake dataset (n=72) comprising a limited number of locations over the world (Ke et al., 2026).

The aim of this study was to investigate the applicability of 3-OH FAs as temperature proxies in lakes at the global scale using an extended dataset (n=241) and refined statistical models. This dataset was obtained by compiling previously published data with 130 additional lakes covering a large range of latitudes, elevations and climate types. Such a dataset allowed to assess for the first time the inter-lake variability of 3-OH FA distribution at the global level and the correlations with environmental factors. In addition to linear models, several machine-learning algorithms were tested to develop global temperature calibrations, including multilinear and random forest models, as suggested by previous 3-OH FA studies (Véquaud et al., 2021; Guria et al., 2026; Ke et al., 2026), as well as the recently established TabPFN model (Hollman et al., 2025). Finally, for a further validation, all models were tested and compared on a sediment core from Lake Blauvelt (Northeast US) spanning the last ca. 2000 years (Hou et al., 2026). This core represents the only lacustrine 3-OH FA-based temperature record available to date.

2. Materials and methods

2.1 Global lacustrine datasets

The global dataset of this study includes published 3-OH FA data from 52 lakes in the French Alps and 20 lakes in southern Chile (Ke et al., 2026), 20 lakes in China (Yang et al., 2021), and 21 lakes along the east coast of the United States (Hou et al., 2026). In addition, new analyses were made by this study, extending this set with 130 surface sediments of lakes distributed across the globe (Fig. 1), with 3-OH FAs eventually detected in 128 of these lakes (and absent in samples with ID 242 and 243, cf. Appendix). The complete 3-OH FA dataset is made of 241 lakes.

The 130 newly analyzed samples are the top 1 or 1.5 cm of lake sediment cores stored at the EDYTEM laboratory repository in Chambéry, France, and the Continental Scientific Drilling Facility (CSD Facility) of the University of Minnesota, the United States. Lakes were selected considering the representativeness of different latitudes and climates. All continents are included, with 13 lakes from Africa, 21 from Asia, 20 from Europe, 25 from South America, 40 from North America, and 11 from Oceania. The latitude of the studied locations spans between 78.05 to -54.63, with a maximum elevation of 5088 m above sea level (Appendix). The MAATs ranged from -14.2°C to 27.7°C, with an average value of 9.9°C (Fig. 2). The temperature, precipitation, and elevation data are obtained from the WorldClim model (Fick and Hijmans, 2017), which is composed of monthly data from 1970 to 2000 at a 1 km resolution. The MAATs and Months Above Freezing (MAF) are calculated as the average temperature of all twelve months, and months above 0°C, respectively. Mean summer temperature (MST) is calculated as mean temperature of June, July, August for latitudes >0, and December, January, February for latitudes <0. The inclusion of the MAF and MST is necessary to investigate the potential seasonal influence on the production of 3-OH FAs by Gram-negative bacteria, as previously suggested for brGDGTs (Deng et al., 2016; De Jonge et al., 2014). The reliability of the WorldClim model has been previously validated by Zhu et al. (2025) who observed a strong and significant the correlation of modeled MAAT with measured values (R^2=0.99, RMSE=1.13°C, $p<0.01$; n=949).

pH data of 120 lakes were collected from the literature for the newly analyzed samples, and from the original publications for the rest of the data (Appendix). pH was comprised between 7.5 and 9 for most of the documented lakes (Fig. 2).

2.2 3-OH FA extraction and analysis

3-OH FAs were extracted and analyzed following Huguet et al. (2019). Briefly, all sediments were frozen and then freeze-dried. Ca. 0.5 g of ground and homogenized sediment sample was first hydrolysed with 30 ml of 3 M HCl under reflux at 130°C for 3 h with magnetic stirring. After cooling, the sample was centrifuged at 15°C and 3000 rpm for 5 minutes. The samples were subsequently

extracted twice with 20 mL of 1:1 dichloromethane (DCM)/methanol and twice with 20 mL DCM by 10-minute ultrasonic bath. Each extraction was followed by centrifugation and collection of the solvent. The organic phase was decanted carefully and re-extracted three times with 20 mL DCM. The extracts were dehydrated with anhydrous sodium sulfate, filtered and then rotary evaporated. Afterwards, the sample was methylated using 10 mL of 1M HCl–MeOH solution at 80°C for 1 h. The lipids were separated through activated silica gel columns into three fractions by polarity: (i) fraction 1, which contained non-OH fatty acid methyl esters (FAMEs), was eluted with 30 mL of 98:2 *n*-heptane/ethyl acetate; (ii) fraction 2, which contained OH FAMEs, was eluted with 30 mL of ethyl acetate; and (iii) fraction 3, which was eluted with 30 mL of methanol. Each fraction was rotary evaporated and N_2 dried after collection.

Before the analysis of 3-OH FAs contained in fraction 2, all the samples were diluted with DCM to a concentration of approximately 2 µg/mL. Each sample was prepared with 50 µL of sample solution, and 50 µL of bis-(trimethylsilyl-) trifluoroacetamide (BSTFA) for silylation at 70°C for one hour. Additionally, 4 µL of internal standard (3-hydroxytetradecanoic acid, 2,2,3,4,4-d5; Sigma–Aldrich, France; 2 µg/mL) was added. The prepared samples were injected into a gas chromatograph coupled to a mass spectrometer (GC–MS TRACE 1310 – ISQ 7000, Thermo Fisher). 1 µL of sample was injected at 280°C in splitless mode. The GC oven was first heated from 70°C to 200°C (10°C/min), then from 200°C to 310°C at a step of 2°C/min, and subsequently stabilized at 310°C for 20 min, with helium used as the carrier gas. 3-OH FAs were identified on the basis of their retention time after extraction of the characteristic *m/z* 175 fragment (*m/z* 178 for the deuterated internal standard; cf. Huguet et al., 2019). The 3-OH FAs were quantified by integrating the appropriate peak on the ion chromatogram and calculating the relative abundance.

2.3 3-OH FA-based temperature proxies

Different indices based on 3-OH FAs were calculated. Thus, the RAN_{15} and RAN_{17} proposed by Wang et al. (2016) as temperature proxies in soils were calculated as follows:

$$RAN_{15} = a\text{-}C_{15}/n\text{-}C_{15} \quad \text{Eq. 1}$$

$$RAN_{17} = a\text{-}C_{17}/n\text{-}C_{17} \quad \text{Eq. 2}$$

a- represents the relative abundance of *anteiso*, and *n*- represents *normal* 3-OH FAs.

In addition, the branched ratio and RIAN, previously suggested as pH proxies in soils by Wang et al. (2016), were calculated as follows:

$$\text{Branched Ratio} = (I+A)/N \quad \text{Eq. 3}$$

$$\text{RIAN} = -\log^{10}(\text{Branched Ratio}) \quad \text{Eq. 4}$$

where *I*, *A*, *and N* represent the sum of the relative abundance of all the *iso*, *anteiso*, and *normal* homologues, respectively.

In addition, Yang et al. (2021) suggested RAN_{13} and RIN_{17} as MAAT proxies in lakes, which are calculated as follows:

$$RAN_{13} = a\text{-}C_{13}/n\text{-}C_{13} \quad \text{Eq. 5}$$

$$RIN_{17} = i\text{-}C_{17}/n\text{-}C_{17} \quad \text{Eq. 6}$$

Four samples were randomly selected and analysed in triplicate to determine the analytical error. The relative standard deviation (RSD) was calculated as follows:

$$RSD = (SD)/ (\bar{x}) * 100\%$$

where SD is the standard deviation, and $\bar{x}$ is the average value of each triplicate.

The average RSD of the triplicates is 3.8% for RAN_{15}, 5.2% for RAN_{17}, 2.0% for the branched ratio, 3.9% for RIAN, 2.2% for RAN_{13} and 5.5% for RIN_{17}.

2.4 Statistical Analysis

All the statistical analyses were conducted using R 4.3.2 (R studio). The Pearson correlation coefficient between 3-OH FA relative abundances/indices and temperatures was calculated using the *Hmisc* package (Harrell Jr, 2003). Principal Component Analysis (PCA) was performed using the package *stringr* (Wickham, 2009). Hierarchical clustering analysis was performed using the function 'hclust'. The function 'fviz_nbclust' in the package *factoextra* was used to determine the optimal number of clusters (Kassambara and Mundt, 2016). Significance of correlations are inferred from *p*-value < 0.05.

2.5 Machine learning models

Three machine learning models were implemented on the global lake 3-OH FA dataset to develop temperature calibrations: random forest (RF), multilinear, and TabPFN. All the models were 10-fold cross-validated to avoid overfitting (Yates et al., 2023), as previously proposed in other machine learning biomarker studies (Pearson et al., 2025; Zhang et al., 2024; Zhou et al., 2026). Briefly, all the models were run 10 times independently. Within each run, 90% of the data were selected as the training set, and the other 10% was selected as the testing set to generate predictions. The dataset was split into a rotating scheme across the 10 runs; therefore, each sample was predicted only one time. We evaluated the models by comparing their temperature predictions to the observed MAAT, MAF, and MST. The R^2 and Root Mean Square Error (RMSE) of the prediction–observation correlations were calculated to

indicate the strength and accuracy of the predictions, respectively. The outliers were selected by the Rosner test (Rosner, 1983) using the package *EnvStats* (Millard et al., 2025) in R 4.3.2.

2.5.1 Random Forest and Multilinear Algorithms

Random forest (RF) and multilinear algorithms were implemented in previous lacustrine and soil 3-OH FA studies aiming to develop temperature calibrations (Ke et al., 2026; Véquaud et al., 2021). Both models included all the individual 3-OH FA homologues. This allows capturing the complexity of the response of Gram-negative bacteria and their whole suite of 3-OH FAs to temperature changes in a linear and non-linear way through the multilinear and RF algorithms, respectively. The multilinear model provides traceable parametric equations but cannot take into account non-linear influences which can occur in environmental settings. This can be overcome using some of the machine learning models such as the RF algorithm. The latter is based on a number of decision trees and hence a forest (Breiman, 2001). After inputting the relative abundances of 3-OH FAs and temperatures of the training dataset (90% of the whole dataset), the models learn the relationship between temperature and each 3-OH FA compound from the training dataset. The rest of the dataset (10%) is used to test the model. As a non-parametric model, the RF cannot be expressed as equations. However, the weight of each individual 3-OH FA in the temperature RF calibration can still be obtained by using the permutation importance method (Breiman, 2001).

Both models were built in R 4.3.2 (R studio) using the *randomForest* and *randomForestExplainer packages* for the RF calibration and the *lm command* for the multilinear model, respectively. To reduce model redundancy, the 3-OH FA homologues having the lowest relative importance were excluded from the RF model. Tests were performed to obtain the model with the strongest determination coefficient (R^2) and smallest RMSE. This led to keep the 15 compounds with the highest weight in the model.

2.5.2 TabPFN models

Most machine-learning models, such as the RF algorithm, are based on decision trees. The training of such models is usually favored by large datasets (e.g., Luan et al., 2020; Han et al., 2021). A very recently established model named TabPFN (Hollman et al., 2025) has shown the advantage of dealing with smaller datasets (n<1000). TabPFN developed a new framework by first introducing pre-trained foundation models into tabular data analysis. In contrast to conventional machine learning models that build the models from scratch, TabPFN is pre-trained by developers on millions of synthetic datasets imitating simple to difficult data rules generated by algorithms with varying noise levels. The accuracy of the TabPFN model has been widely validated in data science (Liu and Ye, 2025; Grinsztajn

et al., 2026) but not yet in earth science research. It should be noted that there is no built-in explainability in TabPFN, in contrast with some other algorithms such as the RF, for which the relative weight of each individual compound in the model can be determined. Therefore, the prediction mechanism of temperatures based on 3-OH FAs in the TabPFN model remains a complete black box. This model is implemented only for practical application purposes.

The TabPFN model was installed and run on Python 3.14 using TabPFNRegressor in the *tabpfn package*. The Python script can be found at the end of this paper.

3. Results

3.1 Distribution of 3-OH FAs across environments

The comparison of the mean relative abundance of 3-OH FAs across different settings – soils, lake and oceans – shows a higher proportion of short-chain homologues (C_{10} to C_{14}), especially *n*-C_{10}, in oceans than in lakes and soils (Fig. 3). On average, the *n*-C_{14} 3-OH FA is the most abundant homologue in soils *vs.* the *n*-C_{16} 3-OH FA in lakes (despite partial overlapping of the standard deviations of the *n*-C_{14}, *n*-C_{16} and *n*-C_{18} compounds; Fig. 3). The *normal* isomers are more abundant than the *iso* and *anteiso* ones among the even-numbered 3-OH FAs, whereas the opposite is observed for the odd-numbered compounds.

Principal Component Analysis (PCA) was performed to further compare the distribution of 3-OH FAs in the different environments using all available data (Fig. 4). The first two PCs explain 49.2% of the total variability. The lake, soil, and ocean data cluster away from each other, indicating a distinct 3-OH FA distribution for each environment. The ocean cluster is classified away from the lake and soils on PC1, while the lake and soil clusters are separated, although partly overlapping, along PC2 (Fig. 4). Some of the compounds are more closely related to one cluster. The *n*-C_{16}, *a*-C_{17}, *a*-C_{15}, *i*-C_{16}, *n*-C_{17} and *i*-C_{14} homologues are pointing to the lake cluster (downwards on PC2), while the *n*-C_{18}, *n*-C_{14}, *i*-C_{17}, *i*-C_{15} and *n*-C_{12} 3-OH FAs are strongly pointing to the soil cluster. In addition, short-chain 3-OH FAs are more closely associated with the negative direction of PC1, i.e. the ocean cluster.

3.2 Hierarchical cluster analysis of 3-OH FAs in global lakes

The 3-OH FAs in global lakes (n=241) were separated into 3 groups based on hierarchical cluster analysis (see Section 2.4). Mean values of the abiotic environmental factors for the three clusters present no significant differences, although the MAF of Cluster 2 and elevation of Cluster 3 are slightly higher than in the other clusters, as indicated by the horizontal bar in Fig. 5. The white box in the center represents the top 25% to 75% of the observations. A wider distribution of the three temperatures

(MAAT, MAF, MST) is observed for Cluster 2. The MAP and pH distribution is similar for the three clusters.

The violin plots of Clusters 2 and 3 have an hourglass shape, with denser distributions for values higher and lower than the mean. Cluster 3 includes more high-elevation sites, although it is not sufficient to characterize this cluster as a high-altitude group. Similarly, Cluster 2 contains more tropical sites than the two other clusters. The distribution map shows that the majority of the samples in Clusters 1 and 3 (Fig. 6) are located in temperate zones, although Cluster 1 also contains two lakes with MAAT>20°C. The distribution of samples from Cluster 2 is much wider across the latitude and longitude ranges. The clustering does not explicitly combine samples in terms of temperature or geographical features. Nevertheless, lakes compiled from previous regional studies were preferentially grouped through cluster analysis, with 18 out of 20 lakes of China (Yang et al., 2021) and 40 out of 52 lakes of the French Alps (Ke et al., 2026) associated to Cluster 3 and15 out of 21 lakes of the East Coast U.S. (Hou et al., 2026) associated to Cluster 1.

A PCA was also performed on the lacustrine 3-OH FA global dataset (n=241) using cluster labeling (Fig. 7). This allows to further visualize and compare the lipid distribution between the clusters. The first two PCs explain 43.6% of the total variability. The three clusters are distributed along PC1, even though Cluster 1 also stands out along PC2. The clusters are partly overlapping, with Cluster 1 associated with long-chain (C_{14} to C_{18}) *iso* compounds but also *n*-C_{15}, *a*-C_{17}, and *n*-C_{17} homologues. Cluster 2 is associated with *a*-C_{15}, *n*-C_{18}, and *n*-C_{16} 3-OH FAs, while Cluster 3 is mainly related with short-chain 3-OH FAs (C_{10} to C_{14}). In addition, the environmental factors (temperatures, pH, elevation, and precipitation data, cf. section 2.1) were also incorporated into the PCA, with the arrows representing the correlation of each factor along the PCs. Temperatures are mainly negatively correlated along PC1, while precipitation and elevation are positively correlated along PC1 and negatively along PC2, and pH is mainly negatively correlated along PC2. This indicates that Cluster 2 includes warmer samples than the other two clusters, while Cluster 3 comprises samples characterized by higher elevation, precipitation and pH.

3.3 Correlations of 3-OH FAs with temperature

The relationships between the individual 3-OH FAs and temperatures (MAAT, MAF and MST) were investigated through a correlation matrix (Fig. 8). The 3-OH FAs have only weak to moderate correlations with temperature (max r=0.5). The correlations of all variables with MST are generally weaker than those with MAAT and MAF. The *i*-C_{13}, *a*-C_{15}, and *n*-C_{18} 3-OH FAs show the strongest correlations with temperature, as also observed through PCA (Fig. 7). Most of the *iso* and *anteiso* compounds are negatively correlated with temperatures, except for the *i*-C_{18} homologue. The mid- and long-chain *normal* isomers are positively correlated with temperature, in contrast with the short-chain

ones (*n*-C_{10}, *n*-C_{11}, and *n*-C_{12}). The Branched ratio, which represents the sum of *iso* and *anteiso* to *normal* homologues (Eq. 3), is negatively correlated with temperature. In contrast, the RIAN index is significantly and positively correlated with temperature and shows stronger correlations than the other indices (RAN_{13}, RAN_{15} and RIN_{17}).

3.4 Machine learning models

Three machine learning models – multilinear and random forest (RF) algorithms and TabPFN – were applied to the lacustrine 3-OH FA dataset to build global temperature calibrations (see Section 2.5). The predicted temperatures are plotted *vs.* the observed values in Fig. 9. Among the three selected models, TabPFN has the strongest correlation and lowest RMSE whatever the temperature tested (MAAT, MAF and MST) and estimates present the smallest offsets from the 1-to-1 line. The MAF predictions of all three models have higher R^2 and lower RMSE than those based on MAAT and MST (Fig. 9). The MST predictions of the TabPFN and RF results have similar R^2 and RMSE values.
The weight of each 3-OH FA in the RF temperature predictions was obtained by calculating the relative importance of every compound using the permutation importance method (Breiman, 2001). The *n*-C_{18} homologue has the highest weight in the three RF temperature models. (Fig. 10). Other homologues (*a*-C_{13}, *n*-C_{13}, *i*-C_{14} and *n*-C_{15} 3-OH FAs) also play important roles in the RF models, with slightly different order depending on the temperature.

4. Discussion

4.1 Sources of the 3-OH FAs in lakes

Aside from environmental factors, different sources of 3-OH FAs can also lead to distinct lipid distributions. Therefore, the sources of the 3-OH FAs in lakes have to be assessed in detail before envisioning a reliable application of these compounds as temperature proxies at the global scale. To this aim, a PCA compiling all the 3-OH FA data available so far for soils, lakes and oceans was performed (Fig. 4) and highlighted distinct 3-OH FA distributions between the three settings. This suggests a prominent contribution of *in situ* production for 3-OH FAs in either the water column or sediments of the lakes. This is consistent with previous regional lake investigations along transects in China (Yang et al., 2021; Wang et al., 2025), the U.S. (Hou et al., 2026), the French Alps, and Chile (Ke et al., 2026), reinforced by higher absolute 3-OH FA concentrations in lakes than in soils of the same region. The

comparison of 3-OH FA concentrations between lakes and soils from the watershed could not be performed at the global scale, as part of the data (3-OH FA abundances in soils and/or TOC contents of soils/sediments) were not available.

Nevertheless, several key features were observed to differentiate the 3-OH FA distribution between lakes and soils. First, *anteiso* homologues are generally more abundant in lakes than soils, with a mean relative abundance of 13.2±5.2% in the global lake dataset (n=241) *vs.* 5.9±2.3% in the global soil one (*n*=309). Such a trend was previously highlighted regionally by Yang et al. (2021), who compared the relative abundance of 3-OH FAs between 20 lake sediments and surrounding soils from China. In addition, Ke et al. (2026) very recently suggested that some individual 3-OH FAs could be used as source indicators either for lakes (namely *i*-C_{14}, *a*-C_{15}, *i*-C_{16}, *n*-C_{16}, and *a*-C_{17} homologues) or soils (namely *n*-C_{14} and *n*-C_{18} isomers). This conclusion, previously obtained from a limited lake dataset (*n*=92; Ke et al. 2026), is strengthened by the present study, with an extended dataset including 149 additional lake samples – 128 newly analyzed (Fig. 4) and 21 from the eastern U.S. (Hou et al., 2026). The higher abundance of the *n*-C_{14} 3-OH FA in soils than in lakes should also be highlighted, as it appears to be the dominant homologue in 268 out of 309 global soils. In contrast, the *n*-C_{16} 3-OH FA is the dominant homologue for 177 out of 241 global lakes, the rest of the samples being dominated by the *n*-C_{14} isomer, possibly related to larger terrestrial influences in corresponding locations.

The different 3-OH FA distribution between soils and lakes may be at least partly related to the distinct Gram-negative bacterial diversity in the two settings, despite some potential overlap (Garner et al., 2023; Haglund et al., 2003; Yannarell and Triplet, 2005). Thus, Wang et al. (2025) recently reported strongly different 3-OH FA distributions and bacterial communities in surface sediments, suspended particulate matter (SPM) and soils surrounding one lake from Central China. Constraining the lipid profiles of Gram-negative bacteria in environmental settings is all the more difficult as the 3-OH FA composition strongly differs from one strain to another (e.g. Edlund et al., 1985, Hellequin et al., 2023). Thus, culture experiments performed on strains of the genus *Pseudomonas*, ubiquitous in soils and lakes (Hong et al., 2008; Elomari et al., 1996; Fang et al., 2011), revealed that the predominant homologues were strain-dependent: the *n*-C_{14} and *n*-C_{16} 3-OH FAs were the most abundant in 3 strains of *P. cepacia* and 2 strains of *P. solanacearum*, while 2 strains of *P. veronii* were dominated by the *n*-C_{10} and *n*-C_{12} isomers (Mora-Gomez et al., 2026). Similarly, the predominant 3-OH FA homologues were shown to differ between strains of the *Bacteroides* genus, commonly found in soils and lakes (Zeng et al., 2026; Baumann et al., 2022), with e.g. the *i*-C_{15} or *a*-C_{15} compounds being the most abundant in the species reported by Mayberry (1980), and the *i*-C_{17} or *n*-C_{16} 3-OH FAs being predominant in those studied by Johne et al. (1988). These examples highlight the diversity of the lipid profile of GNB at the strain level, which is amplified in natural samples. Further studies concomitantly investigating bacterial and lipid diversity are required to better constrain the complex relationships between 3-OH FAs and bacterial producers in environmental settings.

4.2 Interlake diversity of 3-OH FA distributions in global lakes

While inter-setting differences in 3-OH FA distributions are documented and discussed by previous studies (e.g., Yang et al., 2020; Wang et al., 2025; Hou et al., 2026, Ke et al., 2026), the variability in lipid diversity between individual lakes has never been assessed at the global scale before. A cluster analysis was conducted to assess potential regional effects on the distribution of 3-OH FAs, as it could prevent the development of global calibrations between temperature and these lipids. It suggested that the global lacustrine 3-OH FA dataset could be divided into three groups: Cluster 1, dominated by long-chain *iso* homologues; Cluster 2, where the *a*-C_{15}, *n*-C_{16}, and *n*-C_{18} isomers are predominant; Cluster 3, where short-chain 3-OH FAs are the most abundant (Fig. 7). While Cluster 1 and 3 are distributed mainly in temperate zones, Cluster 2 spans large latitudinal ranges. No direct relationship was found between available abiotic factors (temperature, pH, precipitation, and elevation) and 3-OH FA distribution between lakes of the different clusters (Figs. 5 and 6). Nevertheless, it should be noted that several abiotic parameters which could have a key influence on GNB and associated 3-OH FAs are not documented for the present global lake dataset. Among such parameters, Ke et al. (2026) recently showed that the total organic carbon content and, to a lesser extent, the solar radiation and dissolved oxygen content influenced the 3-OH FA distribution in 37 lakes from the French Alps. Similarly, nutrient concentrations (Garner et al., 2023; Mayr et al., 2020) and salinity (Lindström et al., 2005) were previously demonstrated to have an impact on bacterial diversity in lakes and could also influence 3-OH FA distribution. The aforementioned factors, not included in our dataset, could explain part of the 3-OH FA lake clustering.

The variations in terrestrial inputs from one lake to another and their influence on the lipid profiles should also be taken into account. Thus, 26 lakes overlap with the soil samples in the PCA compiling 3-OH FA data from the different settings (Fig. 4). More than half (n=14) of the overlapping lakes belong to Clusters 3, 8 to Cluster 2, and 4 to Cluster 1 (Table S2). A closer look at the lakes of Cluster 3 reveals that allochthonous organic matter is indeed predominant in some of them, such as Lake Lauvitel of the French Alps (Fouinat et al., 2017). Nevertheless, in some other lakes of this cluster (e.g. Lake Melo of the French Alps), a predominant autochthonous origin of organic matter was suggested (Sabatier et al., 2025). Therefore, the impact of terrestrial inputs on the 3-OH FA variability between lakes should be interpreted cautiously and is likely limited. This is supported (i) by the low variance (17.6%) explained per PC2 which separates the soil and lake clusters (Fig. 7) and (ii) by the distribution of the individual 3-OH FAs considered as soil tracers on the basis of the global PCA (Fig. 4) between the 3 lacustrine clusters: the *n*-C_{14} and *n*-C_{12} homologues point to Cluster 3, the *n*-C_{18} 3-OH FA to Cluster 2, and *i*-C_{17} and the *i*-C_{15} 3-OH FAs to Cluster 1 (Fig. 7).

As discussed in section 4.1., changes in bacterial community composition may affect the 3-OH FA distribution and could also explain part of the variability between clusters (Fig. 7). Thus, Wang et al. (2025) compared the diversity of bacterial communities and 3-OH FAs between lake water collected

at three different depths (surface, mi-depth, bottom), surface sediment and soils surrounding Lake Liangzihu in Central China. They observed significant differences in bacterial community and lipid composition between soils and lake sediments on the one hand and the water column on the other hand, supporting lake *in situ* production of 3-OH FAs. Lake SPM were shown to be characterised by higher relative abundances in *i*-$C_{17,}$ *a*-C_{17} and *i*-C_{15} 3-OH FAs and lower relative abundances in short-chain (< C_{14}) *iso* and *anteiso* homologues than in lake sediments and soils (Wang et al., 2025). Such a distribution is consistent with the one observed for lacustrine Cluster 1 (Fig. 7), which might reflect a major contribution of 3-OH FAs produced in the water column for lakes of this cluster. In contrast, Cluster 3 is characterised by a strong signal of short-chain 3-OH FAs (Fig. 7), in line with previous studies in Chinese lakes (Yang et al., 2021; Wang et al., 2025), which highlighted the higher relative abundance of short-chain homologues in sediments than in soils. Cluster 3 might at least partly reflect the production of 3-OH FAs in lake sediments.

Even though a causal link between the changes in lipid distribution and sources between the different lakes may be suggested, the boundaries between the lake clusters are not discrete, with a gradual rather than categorical separation (Fig. 7). In any case, the 3-OH FA distribution in lakes appears generally homogeneous when compared with soil and ocean data (Fig. 4), with modest changes in the regional signals which may reflect variations in lipid sources and microbial diversity. The general independence of the 3-OH FA signal to documented environmental factors supports the applicability of these compounds across lakes with diverse geographic settings, which will be discussed in further detail in the next section.

4.3 Linear correlations of temperature with global lacustrine 3-OH FAs

The inter-lake variability observed in the 3-OH FA distribution may question their applicability as temperature proxies on the global level. Identifying the major compounds involved in the adaptation to temperature among all the homologues is critical to understand the physiological process of the GNB, and consequently improve the robustness of temperature calibrations. 12 out of the 21 3-OH FAs were observed to be significantly ($p<0.05$) correlated with MAAT, MAF, and MST (Fig. 8). Among these 12 compounds, 4 of them – *n*-C_{12}, *i*-C_{13}, *a*-C_{15} and *n*-C_{18} 3-OH FAs – are moderately correlated ($0.3<r<0.6$) with temperature, suggesting that the response of GNB to temperature changes in lakes does not rely on a single, predominant 3-OH FA. Several indices integrating multiple individual 3-OH FAs were previously developed (cf. section 2.2.) and were evaluated as temperature proxies using the present global lake dataset. The RAN_{15} and RAN_{17} (Eqs. 1 and 2) were initially proposed by Wang et al. (2016) as temperature proxies in soils, with a linear increase of these indices with decreasing temperature, consistent with homeoviscous adaptation mechanism (Wang et al., 2016; Huguet et al., 2019). In our global lake dataset the RAN_{15} was significantly but only weakly negatively correlated with temperature

(Fig. 8) while no relationship was observed for the RAN_{17} (Fig. 8). The fact that these two indices cannot be applied as temperature proxies in lakes is consistent with observations previously made at the regional scale (Yang et al., 2021; Hou et al., 2026; Ke et al., 2026) and suggests that Gram-negative bacterial communities in soils and lakes may use different 3-OH FAs to adapt with temperature changes, as previously suggested (e.g. Hou et al., 2026). In this way, the RAN_{13} index (Eq. 5), which was initially proposed as a temperature proxy in marine settings (Yang et al., 2020), was shown to be strongly negatively correlated with temperature in Chinese lakes, as well as more recently in lakes of the Eastern Coast U.S. (Hou et al., 2026), whereas no correlation was observed in lakes from the French Alps and Chile (Ke et al., 2026). In the global lake dataset, this index was only weakly correlated with MAAT, MAF, and MST (R^2<0.3, Fig. 8) with large RMSE (6.6°C to 9.4°C). Similarly, the RIN_{17} (Eq. 6) was shown to be correlated with temperature in Chinese lakes, but in none of the other lacustrine settings investigated (Hou et al., 2026; Ke et al., 2026) nor at the global scale (Fig. 8). Two other indices, the Branched Ratio (Eq. 1) and RIAN (Eq. 2) were first evaluated as pH proxies in soils and appear to be moderately correlated with temperatures in our global dataset (n=241; Fig. 8). Such a correlation is consistent with homeoviscous adaptation, reflected by an increase in the relative abundance of branched homologues at lower temperature to maintain the membrane fluidity and permeability Mansilla et al., 2004; Mostofian et al., 2019; Poger et al., 2014). Nevertheless, the linear relationship between the Branched Ratio or RIAN and the temperature was not observed when lakes were investigated separately (China, Yang et al., 2021; East Coastal U.S., French Alps, Chile), possibly due to the narrow range of temperature variation regionally.

Altogether, our results show the strong regional dependency of the relationship between the different indices based on 3-OH FAs and temperature in lakes, as previously observed in soils (Véquaud et al., 2022). They also highlight the limitations of using a single index defined empirically from only part of the individual lipids to capture the response of these lipids to temperature changes through linear relationships. This appears restrictive and not representative of the environmental complexity, where the bacterial communities and associated membrane lipids are influenced concomitantly and non-linearly by a wide range of (a)biotic factors. Lacustrine bacterial diversity can indeed vary significantly across both temporal and spatial gradients (Lobova et al., 2002; Stabili and Cavallo, 2004; Pontes et al., 2009), which will in turn alter the overall 3-OH FA distribution, independently of any environmental change. In addition, even within taxonomically consistent microbial communities, the distribution of 3-OH FAs in lakes may be influenced by environmental factors other than temperature, including pH, oxygen level, salinity (Garner et al., 2023; Mayr et al., 2020; Lindström et al., 2005) or sedimentary organic carbon content as recently suggested by Ke et al. (2026) in lakes from the French Alps. As a wide range of biotic and abiotic parameters may obscure and weaken the linear relationship between 3-OH FAs and temperature, the development of global lacustrine calibrations has to rely on other models taking into account the specificity and complexity of the lake settings.

4.4 Global temperature calibrations based on machine-learning models

As no strong linear relationship was observed between the individual 3-OH FAs or associated indices and temperatures (Fig. 8), machine-learning approaches that are capable of incorporating all the homologues and/or capturing non-linear relationships between lipid distributions and temperature were applied. Three models, i.e., RF, multilinear and TabPFN, were trained and cross-validated. The multilinear and RF algorithms were shown to be powerful tools in data analysis by previous applications for the development of global 3-OH FA temperature calibration in soils (Véquaud et al., 2021; Guria et al., 2026) and lakes (*n*=72, Ke et al., 2026).

Multilinear regression integrates the linear relationships between all the 3-OH FA homologues and temperature into a single predictive model. When applied to the global lake dataset (*n*=241), the generated predictions of MAAT, MAF, and MST show moderate correlations with observed values (R^2 of 0.51, 0.55, 0.44, respectively) and large offsets (RMSE of 6.73°C, 4.44°C, 5.44°C, respectively; Fig. 9 and Table 1). Even though the multilinear regression (Fig. 9) shows higher determination coefficients with temperatures than the linear correlations based on single 3-OH FAs or derived indices (Fig. 8), its strength and accuracy is systematically lower than the RF and TabPFN models. Once again, this might be due to the intrinsic nature of the multilinear model, which is not able to take into account non-linear influences occurring in complex environmental settings. This limitation can be overcome using non-parametric models, such as the two other machine-learning algorithms proposed in this study, suitable for describing non-linear relationships.

Whatever the temperature, the strength and accuracy of the RF models are slightly higher than those obtained with the multilinear algorithm (Fig. 9 and Table 1). The *n*-C_{18}, *i*-, *a*-, *n*-C_{13}, *a*-C_{15}, and *i*-C_{14} 3-OH FAs, which showed individually weak to moderate linear correlations with temperatures (Fig. 8), were the top contributors of the RF calibrations (Fig. 10), suggesting that they are concomitantly playing a key role in the temperature adaptation of Gram-negative bacteria. The important weight of the three C_{13} isomers in the RF model contrasts with the absence of correlation between the RAN_{13} and temperature in lakes for some regions (Ke et al., 2026; cf. section 4.2) or at the global scale (Fig. 8). Similarly, the a-C_{15} homologue is linearly correlated with temperature (Fig. 8) and one of the main contributors of the RF model (Fig. 10), whereas the RAN_{15}, which was previously proposed as a temperature proxy in soils (Wang et al., 2016; Huguet et al., 2019) does not linearly correlate with temperature in lakes (Fig. 8). Altogether, the RF algorithm highlights the non-linear response of 3-OH FAs to temperature changes, the thermal relevance of some homologues being captured by filtering out non-thermal influences. Nevertheless, the RF global lake calibrations present larger offsets for MAATs below 0°C and for all temperatures beyond 20°C (Fig. 9). The bias of the models at the highest and lowest temperatures might be due to the limited number of samples from warm and cold climates. Although the current dataset spans a large temperature range (Table 1), 188 out of 241 samples were collected in temperate zones (latitude between 22.5°N/S to 66.5°N/S), while only 41 and 12 samples

were from tropical and cold zones, respectively. This may lead to a bias in the prediction towards temperate signals. As the RF model is flexible, this limitation could be easily improved and by analyzing 3-OH FAs in a larger and more representative dataset, including a higher number of samples from tropical and polar regions.

The TabPFN model yields the most promising predictive performance among the three algorithms, displaying the highest strength and accuracy, especially for MAFs (R^2=0.75; RMSE=3.24°C), with small offsets between predicted and observed temperatures (Fig. 9 and Table 1). The TabPFN algorithm is indeed more adapted than the two other models in dealing with small datasets (n<1000) as it does not rely on task-specific training but is pre-trained on millions of synthetic datasets (Hollman et al., 2025) on general tabular data relationships (cf. Section 2.5.2). In addition, the TabPFN takes into account the fact that 3-OH FAs can be concomitantly and non-linearly influenced by environmental parameters including temperature, in contrast with the multilinear regression. The strength and accuracy of the global relationship between 3-OH FAs and MAF based on the TabPFN model (Fig. 9) are comparable to those of the global lake brGDGT-temperature calibrations (Table 1) derived from different machine-learning models, with R^2>0.8 and RMSE<3°C (Martínez-Sosa et al., 2021; Zhu et al., 2025; Pearson et al., 2025). Nevertheless, brGDGT-based calibrations benefit from either larger training datasets (n=949, Zhu et al., 2025; n=349, Pearson et al., 2025) or the use of well-established composite indices such as the MBT'$_{5Me}$ index (Martínez-Sosa et al., 2021), whose the relationship with temperature was largely investigated over the years and validated. In contrast, the current understanding of the mechanistic relationship between 3-OH FAs and temperature remains limited and no composite index equivalent to the MBT'$_{5Me}$ and applicable at the global scale currently exists for 3-OH FAs. Incorporating the full suite of individual lipids into machine-learning models still appears more representative of the complexity of environmental settings than those based on a single index as previously suggested (e.g. Dunkley et al., 2020; Wang et al., 2020; Véquaud et al., 2022) but the corresponding calibrations may integrate redundant predictors and result in larger offsets. In any case, our study highlights the interest of using distinct and complementary statistical approaches to develop global lake 3-OH FA-temperature calibrations, as previously observed for brGDGTs (e.g. Pearson et al., 2025; Zhu et al., 2025).

Whatever the model (multilinear, random forest or TabPFN) used to describe the relationship between 3-OH FAs and temperature in the global lake dataset, the strongest correlations and highest accuracy are observed for MAF predictions (Fig. 8). This suggests an influence of the seasonality on 3-OH FA production, as the mean temperature of months above freezing (MAF) excludes all months than have an average temperature above 0°C, during which the activity of bacteria is assumed to be strongly reduced (e.g. Henriikka Kivilä et al., 2023). Temperature is also expected to affect bacterial community composition in lakes (Adams et al., 2010) and thus potentially 3-OH FA distribution. The prevalence of lakes from temperate and cold regions in our global dataset (200 out 249 samples; Figs. 1 and 2), where

seasonality is expected to be higher, may further strengthen the overall better performance of the calibrations based on MAF rather than MAAT or MST (Fig. 8), as previously suggested for brGDGT calibrations (Martínez-Sosa et al., 2021; Zhu et al., 2025; Pearson et al., 2025).

Even though there is no direct evidence of the effect of thermal regime on 3-OH FA distribution and abundance, a parallel can be drawn with brGDGTs, as the seasonality of production of these lipids was the object of several publications and contrasting observations. Thus, in mid-latitude soils, no effect of seasonal temperature variations on brGDGT production was reported (Weijers et al., 2011; Lei et al., 2016). In contrast, a strong seasonal dependence of brGDGT signals has been reported in several studies investigating soils (e.g. Huguet et al., 2013; Dang et al., 2016) or lakes (e.g. Dang et al., 2018; Cao et al. 2020) from higher latitudes or elevations. Raberg et al. (2021) notably reported stronger correlations of brGDGT fractional abundances with MAF than with either MAAT or MST in the Arctic region (n=43), supporting the fact that brGDGTs may be preferentially produced during non-freezing seasons. Nevertheless, the response of brGDGTs to seasonality is complex, as it was shown to be lake-dependent based on a recent regional study performed in Central Europe (Bauersachs et al., 2024). Similarly to brGDGTs, the influence of seasonality on 3-OH FA distribution and concentration could lead to the strongest correlations observed for MAF than for MAAT or MST (Fig. 8). Detailed investigations of the effects of seasonality on Gram-negative bacterial diversity and 3-OH FAs in lakes from different latitudes are required to confirm such a hypothesis.

Table 1. Comparisons of global temperature calibrations of lacustrine 3-OH FAs (this study) and brGDGTs.

Calibrations	Variables	*n* of samples	R^2	RMSE (°C)	lower limit (°C)	upper limit (°C)
TabPFN-MAAT	3-OH FAs	241	0.69	5.29	-14.3	27.7
TabPFN-MAF	3-OH FAs	241	0.75	3.24	2.4	27.7
TabPFN-MST	3-OH FAs	241	0.58	4.54	-3.3	30.5
RF-MAAT	3-OH FAs	241	0.58	6.24	-14.3	27.7
RF-MAF	3-OH FAs	241	0.61	4.15	2.4	27.7
RF-MST	3-OH FAs	241	0.58	4.69	-3.3	30.5
Multilinear-MAAT	3-OH FAs	241	0.51	6.73	-14.3	27.7
Multilinear-MAF	3-OH FAs	241	0.55	4.44	2.4	27.7
Multilinear-MST	3-OH FAs	241	0.44	5.44	-3.3	30.5
PearsonSC-MST	brGDGTs	349	0.77	5.06	-2.2	31.2
PearsonDC-MST	brGDGTs	349	0.78	3.93	-2.2	30.8
Zhu1-MAF	brGDGTs	775	0.86	2.65	0.8	29.2
Zhu2-MAF	brGDGTs	775	0.89	2.33	0.8	29.2
Zhu3-MAF	brGDGTs	775	0.89	2.27	0.8	29.2
Zhu4-MAF	brGDGTs	775	0.91	2.27	0.8	29.2
Zhu5-MAF	brGDGTs	775	0.92	2	0.8	29.2
Zhu6-MAF	brGDGTs	949	0.8	3.09	0.8	29.2
Martínez-Sosa-MAF	brGDGTs	272	0.88	2.68	1.6	28.1

4.5 Palaeoclimate reconstruction using the 3-OH FA models

While cross-validation suggests the strongest correlation of TabPFN-MAF predictions with observations, the performance and validity of the different models were further tested and compared with the only lacustrine 3-OH FA paleo-record available so far (Hou et al., 2026). This archive was collected from Lake Blauvelt (Northeastern U.S., ca. 50 km away from New York City). The modern air temperature in the area varies widely, with an MAAT of 10.6°C, an average temperature of 21.7°C in summer but only -0.9°C in winter, and a MAF of 13.1°C. The sedimentary core collected in Lake Blauvelt spans the last 2000 years and was analyzed for 3-OH FAs (8 samples) and brGDGTs (9 samples; Hou et al., 2026). Local temperature calibrations of the RAN_{13} and MBT'_{5Me} indices in U.S. East Coast lakes were previously developed by Hou et al. (2026) to consider the specific brGDGT and 3-OH FA distributions in lakes of this region compared to global datasets. The temperature reconstructions derived from these local calibrations will be compared with those obtained from the global 3-OH FA temperature models proposed in the present study (cf. previous section).

The temperature variations of MAAT and MAF reconstructed over the last 2000 yrs using our 3-OH FA global calibration models are very large (ca. 10°C; Figs. 11a and c), and far too excessive, as the amplitude of MAAT during the Holocene is expected to be up to ca. 2–3 °C (Liu et al., 2014). In addition, the offset with modern MAAT and MAF is much higher (>7°C) than the RMSE from the cross-validation (3 to 4°C; Fig. 9). This shows that the global 3-OH FA models do not provide reliable MAAT and MAF reconstructions from the Lake Blauvelt archive. Similarly, the MAF reconstructed from brGDGT global calibrations (Martínez-Sosa et al., 2021; Zhu et al., 2025) are as warm as those derived from 3-OH FAs (Fig. 11c), highlighting consistent regional effects on lipid distribution in Lake Blauvelt.

In contrast with MAAT and MAF, the MST reconstructions based on the global RF and TabPFN models (Fig. 11e) are in agreement with the temperatures derived from the regional RAN_{13} and MBT'_{5Me} calibrations (Fig. 11f). The variability of the MST derived from these two algorithms over the last 2000 yrs is limited (ca. 3°C for the RF and TabPFN) and falls within the calibrations error (Fig. 9 and 11e). Moreover, the TabPFN-MST reconstruction recorded a temperature drop below modern values during the Little Ice Age period (LIA, ca. 1550 to 1850 CE), consistent with current knowledge that the temperature warmed back after LIA towards present with the beginning of the industrialization (Bradley and Jones, 1993). In contrast, the fact that the present-day MST reconstructed from the global multilinear model (18°C) is lower than the recorded value (21.7°C; Fig. 11e) and the high amplitude of MST reconstructed during the LIA question the reliability of this calibration for MST reconstruction in Lake Blauvelt. Altogether, our results highlight the potential of the global RF and TabPFN algorithms for MST reconstructions in Lake Blauvelt and could suggest a bias towards a stronger summer signal in this location. This is supported by the fact that the MAAT estimates derived from either the global 3-OH FA models (Fig. 11a) and regional RAN_{13} calibration (Fig. 11b) are much higher than instrumental MAAT.

In order to consider the potential regional effects on lipid distribution, regional models were trained from the 21 lakes of Eastern Coastal U.S. (Hou et al., 2026) using the same algorithms as those previously applied to the global 3-OH FA dataset (i.e. multilinear regression, RF, and TabPFN). The results of the regional multilinear regression model will not be discussed, as the corresponding temperature estimates were out of range, likely due to the fact that the size of the dataset was too small to make this algorithm reliable. The MAAT, MAF and MST reconstructed from the regional RF and TabPFN models are consistent with modern values, with a difference of ca. 2°C (Figs. 11b, d and f). In addition, the MAAT and MAF records derived from the regional TabPFN model (Figs. 11b and d) are in close agreement with those obtained from the RAN_{13} and MBT'_{5Me} indices (Hou et al., 2026), while the regional RF-derived MAAT and MAF estimates are systematically lower than those derived from the other calibrations but closer to modern instrumental values (Figs. 11b and d). Nevertheless, when considering the uncertainty calibration ranges, the four regional models appear to perform comparably. The RAN_{13}, TabPFN and RF models tend to show a decrease of the MAF over the last 2000 yrs (the last century is not recorded by this core, Fig. 11d). This cooling trend is consistent with regional records and is likely driven by solar radiation, as discussed by Hou et al. (2026). In contrast with the other models, the MBT'_{5Me}-derived MAF shows a slight increase between 0 and 1500 yr cal CE (Fig. 11d), which could be due to seasonal and/or ecological differences in 3-OH FA and brGDGT production in Lake Blauvelt (Hou et al., 2026). However, all the regional models fail to reconstruct the expected temperature drop at the LIA and display a warmer temperature than today (Figs. 11b and d), contrasting with current records (Bradley and Jones, 1993), which could be due to the limited sample size of the regional training dataset. In addition to MAF and MAAT, MST was also reconstructed using regional TabPFN and RF models (Fig. 11f), with results comparable to those obtained from global calibrations (Fig. 11e). This might suggest that summer conditions impose similar pressures across lakes at the global scale, reducing location-dependent variability of 3-OH FA signature, in contrast with year-round observations.

In summary, regional 3-OH FA models based on machine-learning algorithms appeared to be more suitable than global calibrations when applied to MAF and MAAT reconstruction, as they consider the specific adaptations of microbial communities and associated membrane lipids to environmental parameters. Such a lake with a strong regional signature may fall out of the representativeness of our global dataset, as global calibrations may suppress regional responses to climatic variations. However, the present results do not preclude the use of the global 3-OH FA models for temperature reconstruction. This includes Lake Blauvelt, where the regional signal is weakened in summer signals, allowing the global TabPFN and RF model to reconstruct a drastic MST drop during the LIA (Fig. 11e), absent in the records from the regional models (Fig. 11f). Global calibrations present the advantage of capturing a wide range of natural variability and are designed to be used directly, by reflecting an averaged variation pattern of lacustrine lipid to temperature changes. In contrast, geographically-restricted calibrations are limited in universal applications, with applicability boundaries often unclear. In any case,

679 the present results show the potential of RF and TabPFN algorithms to develop regional and global
680 calibrations capturing the non-linear response of 3-OH FAs to temperature variations in lacustrine
681 settings. The global temperature calibrations for 3-OH FAs proposed in the present study could be
682 further improved by expanding and maximizing the representability of the dataset in terms of
683 temperature gradients and environmental conditions.

684

685 # 5. Conclusions

686 This study evaluated the applicability of 3-OH FAs as temperature proxies in lakes using an
687 extended dataset comprising 241 samples from all over the world, including 128 newly analyzed surface
688 sediments. The statistical comparison of the 3-OH FA distribution in global soils, lakes, and marine
689 sediments highlighted the major contribution of *in situ* production in lacustrine settings. Interlake
690 variations in lipid distribution were identified by hierarchical clustering analysis, leading to the
691 separation of the global dataset into 3 groups with no discrete separation. This suggests only modest
692 differences in 3-OH FA signature between these clusters, likely reflecting variations in lipid sources
693 and/or microbial diversity with general independence of the 3-OH FA signal to climatic forcing.

694 Only weak linear correlations between the relative abundances of 3-OH FAs, including
695 previously proposed indices such as the RAN_{13} index, and the temperatures (MAAT, MAF, and MST)
696 were observed in the global lacustrine dataset. Three other models – multiple linear regression, random
697 forest (RF), and TabPFN algorithms – were tested and provided stronger correlations with temperatures,
698 especially the RF and TabPFN, which take into account the fact that 3-OH FAs can be concomitantly
699 and non-linearly influenced by environmental parameters including temperature. The TabPFN-based
700 MAF predictions especially showed comparable strength (R^2=0.75) and accuracy (RMSE=3.24°C) to
701 global lacustrine temperature calibrations based on brGDGTs.

702 The applicability of the global lacustrine calibrations were tested on a lacustrine sediment
703 record from Lake Blauvelt (Eastern U.S.) and compared with regional calibrations developed using the
704 same algorithms. The MAAT and MAF reconstructed from both RF and TabPFN regional models
705 presented better reliability than global ones, likely due to the fact that the regional calibrations consider
706 the specific adaptations of microbial communities and associated membrane lipids to environmental
707 parameters. In contrast, the global models based on the RF and TabPFN algorithms showed potential
708 for MST reconstructions, the TabPFN model especially recording an expected temperature drop over
709 the Little Ice Age, absent in all regional models. Hence, the present results do not preclude the use of
710 the global 3-OH FA models for temperature construction, as geographically-restricted calibrations take
711 into account regional effects but are limited in universal applications, with applicability boundaries often
712 unclear. The new global models can be easily improved through the Python and R scripts available

online and could be extended with samples from warm and cold regions to increase the representativeness of the global lacustrine dataset, where temperate sediments are presently predominant. This study demonstrates the major potential of 3-OH FAs as temperature proxies in lacustrine settings through the use of machine-learning algorithms.

Acknowledgements

The authors acknowledge the Continental Scientific Drilling (CSD) Facility and EDYTEM repository for their assistance in sample collection. In addition, we would like to thank the Elsevier Research Scholarship and the Visiting Graduate Student Program of the CSD facility (National Science Foundation - Instrumentation and Facilities Program; EAR-1951112) for the support of the travel costs of Sai Ke for core sampling.

Funding sources

This work was supported by the French National Research Agency (ANR) [grant number ANR-22-CE01-0002].

Author contributions: CRediT

Sai Ke: Writing – original draft, Visualization, Validation, Software, Methodology, Investigation, Formal analysis, Conceptualization. **Pierre Sabatier:** Validation, Methodology, Conceptualization. **Christelle Anquetil:** Investigation, Validation. **Arnaud Huguet:** Validation, Supervision, Resources, Project administration, Methodology, Funding acquisition, Conceptualization. All the authors have contributed to the review and editing of the manuscript.

Code and data availability

The scripts of the codes of the machine-learning models and associated information can be found at https://doi.org/10.5281/zenodo.21410590

The 3-OH FA lacustrine data will be added to Pangaea.

References

Adams, H.E., Crump, B.C., Kling, G.W., 2010. Temperature controls on aquatic bacterial production and community dynamics in arctic lakes and streams. Environmental Microbiology 12, 1319–1333. https://doi.org/10.1111/j.1462-2920.2010.02176.x

Bailey, C., Gwyther, P., Čaušević, S., Greene, B.L., Van Der Meer, J.R., 2025. Phosphite as an engineered niche for Pseudomonas veronii in a synthetic soil bacterial community. mSystems 10, e00061-25. https://doi.org/10.1128/msystems.00061-25

Baker, J.M., Vander Schaaf, N.A., Cunningham, A.M.G., Hang, A.C., Reeves, C.L., Huffman, E.R., Riester, C.J., Madigan, M.T., Sattley, W.M., 2019. Chemoorganotrophic Bacteria From Lake Fryxell, Antarctica, Including Pseudomonas Strain LFY10, a Cold-Adapted, Halotolerant Bacterium Useful in Teaching Labs. Front. Microbiol. 10, 156. https://doi.org/10.3389/fmicb.2019.00156

Batrich, M., Maskeri, L., Schubert, R., Ho, B., Kohout, M., Abdeljaber, M., Abuhasna, A., Kholoki, M., Psihogios, P., Razzaq, T., Sawhney, S., Siddiqui, S., Xoubi, E., Cooper, A., Hatzopoulos, T., Putonti, C., 2019. Pseudomonas Diversity Within Urban Freshwaters. Front. Microbiol. 10, 195. https://doi.org/10.3389/fmicb.2019.00195

Bauersachs, T., Schubert, C.J., Mayr, C., Gilli, A., Schwark, L., 2024. Branched GDGT-based temperature calibrations from Central European lakes. Science of The Total Environment 906, 167724. https://doi.org/10.1016/j.scitotenv.2023.167724

Baumann, K.B.L., Thoma, R., Callbeck, C.M., Niederdorfer, R., Schubert, C.J., Müller, B., Lever, M.A., Bürgmann, H., 2022. Microbial Nitrogen Transformation Potential in Sediments of Two Contrasting Lakes Is Spatially Structured but Seasonally Stable. mSphere 7, e01013-21. https://doi.org/10.1128/msphere.01013-21

Bittner, L., De Jonge, C., Gil-Romera, G., Lamb, H.F., Russell, J.M., Zech, M., 2022. A Holocene temperature (brGDGT) record from Garba Guracha, a high-altitude lake in Ethiopia. Biogeosciences 19, 5357–5374. https://doi.org/10.5194/bg-19-5357-2022

Bradley, R.S., Jones, P.D., 1993. "Little Ice Age" summer temperature variations: their nature and relevance to recent global warming trends. The Holocene 3, 367–376. https://doi.org/10.1177/095968369300300409

Breiman, L., 2001. Random Forests. Machine Learning 45, 5–32. https://doi.org/10.1023/A:1010933404324

Cao, J., Rao, Z., Shi, F., Jia, G., 2020. Ice formation on lake surfaces in winter causes warm-season bias of lacustrine brGDGT temperature estimates. Biogeosciences 17, 2521–2536. https://doi.org/10.5194/bg-17-2521-2020

Castañeda, I.S., Schouten, S., 2011. A review of molecular organic proxies for examining modern and ancient lacustrine environments. Quaternary Science Reviews 30, 2851–2891. https://doi.org/10.1016/j.quascirev.2011.07.009

Cerri, C.E.P., Sparovek, G., Bernoux, M., Easterling, W.E., Melillo, J.M., Cerri, C.C., 2007. Tropical agriculture and global warming: impacts and mitigation options. Sci. agric. (Piracicaba, Braz.) 64, 83–99. https://doi.org/10.1590/S0103-90162007000100013

Chen, Y., Zheng, F., Yang, H., Yang, W., Wu, R., Liu, X., Liang, H., Chen, H., Pei, H., Zhang, C., Pancost, R.D., Zeng, Z., 2022. The production of diverse brGDGTs by an Acidobacterium providing a physiological basis for paleoclimate proxies. Geochimica et Cosmochimica Acta 337, 155–165. https://doi.org/10.1016/j.gca.2022.08.033

Dang, X., Ding, W., Yang, H., Pancost, R.D., Naafs, B.D.A., Xue, J., Lin, X., Lu, J., Xie, S., 2018. Different temperature dependence of the bacterial brGDGT isomers in 35 Chinese lake sediments compared to that in soils. Organic Geochemistry 119, 72–79. https://doi.org/10.1016/j.orggeochem.2018.02.008

De Jonge, C., Radujković, D., Sigurdsson, B.D., Weedon, J.T., Janssens, I., Peterse, F., 2019. Lipid biomarker temperature proxy responds to abrupt shift in the bacterial community composition

in geothermally heated soils. Organic Geochemistry 137, 103897. https://doi.org/10.1016/j.orggeochem.2019.07.006

De Jonge, C., Hopmans, E.C., Zell, C.I., Kim, J.-H., Schouten, S., Sinninghe Damsté, J.S., 2014. Occurrence and abundance of 6-methyl branched glycerol dialkyl glycerol tetraethers in soils: Implications for palaeoclimate reconstruction. Geochimica et Cosmochimica Acta 141, 97–112. https://doi.org/10.1016/j.gca.2014.06.013

Dearing Crampton-Flood, E., Tierney, J.E., Peterse, F., Kirkels, F.M.S.A., Sinninghe Damsté, J.S., 2020. BayMBT: A Bayesian calibration model for branched glycerol dialkyl glycerol tetraethers in soils and peats. Geochimica et Cosmochimica Acta 268, 142–159. https://doi.org/10.1016/j.gca.2019.09.043

Deng, L., Jia, G., Jin, C., Li, S., 2016. Warm season bias of branched GDGT temperature estimates causes underestimation of altitudinal lapse rate. Organic Geochemistry 96, 11–17. https://doi.org/10.1016/j.orggeochem.2016.03.004

Diffenbaugh, N.S., Singh, D., Mankin, J.S., Horton, D.E., Swain, D.L., Touma, D., Charland, A., Liu, Y., Haugen, M., Tsiang, M., Rajaratnam, B., 2017. Quantifying the influence of global warming on unprecedented extreme climate events. Proc. Natl. Acad. Sci. U.S.A. 114, 4881–4886. https://doi.org/10.1073/pnas.1618082114

Dunkley Jones, T., Eley, Y.L., Thomson, W., Greene, S.E., Mandel, I., Edgar, K., Bendle, J.A., 2020. OPTiMAL: a new machine learning approach for GDGT-based palaeothermometry. Clim. Past 16, 2599–2617. https://doi.org/10.5194/cp-16-2599-2020

Elomari, M., Coroler, L., Izard, D., LECLERCl, H., 1996. DNA Relatedness among Pseudomonas Strains Isolated from Natural Mineral Waters and Proposal of Pseudornonas veronii sp. nov.

Fang, Y., Xie, G., Lou, M., Li, B., Muhammad, I., 2011. Diversity analysis of Burkholderia cepacia complex in the water bodies of West Lake, Hangzhou, China. J Microbiol. 49, 309–314. https://doi.org/10.1007/s12275-011-0267-2

Garner, R.E., Kraemer, S.A., Onana, V.E., Fradette, M., Varin, M.-P., Huot, Y., Walsh, D.A., 2023. A genome catalogue of lake bacterial diversity and its drivers at continental scale. Nat Microbiol 8, 1920–1934. https://doi.org/10.1038/s41564-023-01435-6

Grinsztajn, L., Flöge, K., Key, O., Birkel, F., Jund, P., Roof, B., Jäger, B., Safaric, D., Alessi, S., Hayler, A., Manium, M., Yu, R., Jablonski, F., Hoo, S.B., Garg, A., Robertson, J., Bühler, M., Moroshan, V., Purucker, L., Cornu, C., Wehrhahn, L.C., Bonetto, A., Schölkopf, B., Gambhir, S., Hollmann, N., Hutter, F., 2026. TabPFN-2.5: Advancing the State of the Art in Tabular Foundation Models. https://doi.org/10.48550/arXiv.2511.08667

Guria, U.N., Samantaray, S., Sen, R., Kumar, V., Dasgupta, B., Ghosh, M., Sanyal, P., 2026. Distributions of membrane lipids (3-hydroxy fatty acids and brGDGTs) in the Eastern Himalayan soil and their global context: insights into temperature and pH variations. Organic Geochemistry 105229. https://doi.org/10.1016/j.orggeochem.2026.105229

Häggi, C., Naafs, B.D.A., Silvestro, D., Bertassoli, D.J., Akabane, T.K., Mendes, V.R., Sawakuchi, A.O., Chiessi, C.M., Jaramillo, C.A., Feakins, S.J., 2023. GDGT distribution in tropical soils and its potential as a terrestrial paleothermometer revealed by Bayesian deep-learning models. Geochimica et Cosmochimica Acta 362, 41–64. https://doi.org/10.1016/j.gca.2023.09.014

Haglund, A.-L., Lantz, P., TÃ¶rnblom, E., Tranvik, L., 2003. Depth distribution of active bacteria and bacterial activity in lake sediment. FEMS Microbiology Ecology 46, 31–38. https://doi.org/10.1016/S0168-6496(03)00190-9

Halamka, T.A., Raberg, J.H., McFarlin, J.M., Younkin, A.D., Mulligan, C., Liu, X., Kopf, S.H., 2023. Production of diverse brGDGTs by Acidobacterium Solibacter usitatus in response to temperature, pH, and O2 provides a culturing perspective on br GDGT proxies and biosynthesis. Geobiology 21, 102–118. https://doi.org/10.1111/gbi.12525

Hammarlund, D., Barnekow, L., Birks, H.J.B., Buchardt, B., Edwards, T.W.D., 2002. Holocene changes in atmospheric circulation recorded in the oxygen-*n*-isotope stratigraphy of lacustrine

carbonates from northern Sweden. The Holocene 12. https://doi.org/10.1191/0959683602hl548rp
Han, S., Williamson, B.D., Fong, Y., 2021. Improving random forest predictions in small datasets from two-phase sampling designs. BMC Med Inform Decis Mak 21, 322. https://doi.org/10.1186/s12911-021-01688-3
Harrell Jr, F.E., 2003. Hmisc: Harrell Miscellaneous. https://doi.org/10.32614/CRAN.package.Hmisc
Hayashi, N.R., Ishida, T., Yokota, A., Kodama, T., Igarashi, Y., 1999. Hydrogenophilus thermoluteolus gen. nov., sp. nov., a thermophilic, facultatively chemolithoautotrophic, hydrogen-oxidizing bacterium. International Journal of Systematic and Evolutionary Microbiology 49, 783–786. https://doi.org/10.1099/00207713-49-2-783
Hellequin, E., Collin, S., Seder-Colomina, M., Véquaud, P., Anquetil, C., Kish, A., Huguet, A., 2023. Membrane lipid adaptation of soil Bacteroidetes isolates to temperature and pH. Front. Microbiol. 14, 1032032. https://doi.org/10.3389/fmicb.2023.1032032
Hollmann, N., Müller, S., Purucker, L., Krishnakumar, A., Körfer, M., Hoo, S.B., Schirrmeister, R.T., Hutter, F., 2025. Accurate predictions on small data with a tabular foundation model. Nature 637, 319–326. https://doi.org/10.1038/s41586-024-08328-6
Hong, J.C., Momol, M.T., Jones, J.B., Ji, P., Olson, S.M., Allen, C., Perez, A., Pradhanang, P., Guven, K., 2008. Detection of Ralstonia solanacearum in Irrigation Ponds and Aquatic Weeds Associated with the Ponds in North Florida. Plant Disease 92, 1674–1682. https://doi.org/10.1094/PDIS-92-12-1674
Hou, C., Griffiths, M.L., Hardman, A., Seki, O., Zhou, A., Greene, S., Patterson, E.W., Indriksons, R., Ryan, S., DaSilva, M., Allison, M., Chen, L., Li, M., Bendle, J., 2026. 3-OH-FA- and branched GDGT-based temperature calibrations from a transect of lakes in the eastern USA. Organic Geochemistry 105137. https://doi.org/10.1016/j.orggeochem.2026.105137
Hou, X., Wang, N., Sun, Z., Yuan, K., Cao, X., Hou, J., 2024. BrGDGT-based seasonal paleotemperature reconstruction for the last 15 000 years from a shallow lake on the eastern Tibetan Plateau. Clim. Past 20, 335–348. https://doi.org/10.5194/cp-20-335-2024
Huguet, A., Coffinet, S., Roussel, A., Gayraud, F., Anquetil, C., Bergonzini, L., Bonanomi, G., Williamson, D., Majule, A., Derenne, S., 2019. Evaluation of 3-hydroxy fatty acids as a pH and temperature proxy in soils from temperate and tropical altitudinal gradients. Organic Geochemistry 129, 1–13. https://doi.org/10.1016/j.orggeochem.2019.01.002
Huguet, A., Fosse, C., Laggoun-Défarge, F., Delarue, F., Derenne, S., 2013. Effects of a short-term experimental microclimate warming on the abundance and distribution of branched GDGTs in a French peatland. Geochimica et Cosmochimica Acta 105, 294–315. https://doi.org/10.1016/j.gca.2012.11.037
Johne, B., Olson, I., Bryn, K., 1988. Fatty acids and sugars in lipopolysaccharides from Bacteroides intermedius, Bacteroides gingivalis and *Bacteroides loescheii*. Oral Microbiology and Immunology 3, 22–27. https://doi.org/10.1111/j.1399-302X.1988.tb00600.x
Kassambara, A., Mundt, F., 2016. factoextra: Extract and Visualize the Results of Multivariate Data Analyses. https://doi.org/10.32614/CRAN.package.factoextra
Ke, S., Sabatier, P., Contreras, S., Lemarié, J., Cosyn-Wexsteen, L., Cerda-Peña, C., Giguet-Covex, C., Messager, E., Julien, A., Begorre, C., Huguet, A., 2026. Evaluation of bacterial membrane lipids (3-hydroxy fatty acids and branched GDGTs) as environmental proxies in lakes of the French Alps and southern Chile. Organic Geochemistry 216, 105138. https://doi.org/10.1016/j.orggeochem.2026.105138
Lehtonen, H., 1996. Potential effects of global warming on northern European freshwater fish and fisheries. Fisheries Management Eco 3, 59–71. https://doi.org/10.1111/j.1365-2400.1996.tb00130.x
Lei, Y., Yang, H., Dang, X., Zhao, S., Xie, S., 2016. Absence of a significant bias towards summer temperature in branched tetraether-based paleothermometer at two soil sites with contrasting

temperature seasonality. Organic Geochemistry 94, 83–94. https://doi.org/10.1016/j.orggeochem.2016.02.003
Liang, J., Chevalier, M., Liu, K., Perfumo, A., Wang, M., Xie, H., Hou, J., Herzschuh, U., Chen, F., 2024. Discrepancies in lacustrine bacterial lipid temperature reconstructions explained by microbial ecology. Commun Earth Environ 5, 759. https://doi.org/10.1038/s43247-024-01925-3
Lindström, E.S., Kamst-Van Agterveld, M.P., Zwart, G., 2005. Distribution of Typical Freshwater Bacterial Groups Is Associated with pH, Temperature, and Lake Water Retention Time. Appl Environ Microbiol 71, 8201–8206. https://doi.org/10.1128/AEM.71.12.8201-8206.2005
Liu, S.-Y., Ye, H.-J., 2025. TabPFN Unleashed: A Scalable and Effective Solution to Tabular Classification Problems. https://doi.org/10.48550/arXiv.2502.02527
Lobova, T.I., Maksimova, E.Y., Popova, L.Y., Pechurkin, N.S., 2002. Geographical and seasonal distribution of multiple antibiotic resistance of heterotrophic bacteria of Lake Shira. Aquatic Ecology 36, 299-307. https://doi.org/10.1023/A:1015618820450
Loomis, S.E., Russell, J.M., Ladd, B., Street-Perrott, F.A., Sinninghe Damsté, J.S., 2012. Calibration and application of the branched GDGT temperature proxy on East African lake sediments. Earth and Planetary Science Letters 357–358, 277–288. https://doi.org/10.1016/j.epsl.2012.09.031
Lotter, A.F., Birks, H.J.B., Hofmann, W., Marchetto, A., 1997. Modern diatom, cladocera, chironomid, and chrysophyte cyst assemblages as quantitative indicators for the reconstruction of past environmental conditions in the Alps. Journal of Palelimnology 18, 395-420. https://doi.org/10.1023/A:1007982008956
Luan, J., Zhang, C., Xu, B., Xue, Y., Ren, Y., 2020. The predictive performances of random forest models with limited sample size and different species traits. Fisheries Research 227, 105534. https://doi.org/10.1016/j.fishres.2020.105534
Makiewicz, A., Ratajczak, W., 1993. PRINCIPAL COMPONENTS ANALYSIS (PCA). Computers and Geosciences 19, 303-342. https://doi.org/10.1016/0098-3004(93)90090-R
Malcolm, J.R., Liu, C., Neilson, R.P., Hansen, L., Hannah, L., 2006. Global Warming and Extinctions of Endemic Species from Biodiversity Hotspots. Conservation Biology 20, 538–548. https://doi.org/10.1111/j.1523-1739.2006.00364.x
Mansilla, M.C., Cybulski, L.E., Albanesi, D., De Mendoza, D., 2004. Control of Membrane Lipid Fluidity by Molecular Thermosensors. J Bacteriol 186, 6681–6688. https://doi.org/10.1128/JB.186.20.6681-6688.2004
Martínez-Sosa, P., Tierney, J.E., Stefanescu, I.C., Dearing Crampton-Flood, E., Shuman, B.N., Routson, C., 2021. A global Bayesian temperature calibration for lacustrine brGDGTs. Geochimica et Cosmochimica Acta 305, 87–105. https://doi.org/10.1016/j.gca.2021.04.038
Mayberry, W.R., 1980. Hydroxy fatty acids in Bacteroides species: D-(--)-3-hydroxy-15-methylhexadecanoate and its homologs. J Bacteriol 143, 582–587. https://doi.org/10.1128/jb.143.2.582-587.1980
Mayr, M.J., Zimmermann, M., Guggenheim, C., Brand, A., Bürgmann, H., 2020. Niche partitioning of methane-oxidizing bacteria along the oxygen–methane counter gradient of stratified lakes. The ISME Journal 14, 274–287. https://doi.org/10.1038/s41396-019-0515-8
Millard, S.P., 2013. EnvStats: Package for Environmental Statistics, Including US EPA Guidance. https://doi.org/10.32614/CRAN.package.EnvStats
Mora-Gomez, J., Collin, S., Kish, A., Anquetil, C., Suzuki, M.T., Sabatier, P., Malet, E., Rapuc, W., Begorre, C., Dellinger, M., Huguet, A., 2026. Effect of temperature on membrane lipids of Pseudomonas veronii isolated from French alpine lakes. Organic Geochemistry 217, 105189. https://doi.org/10.1016/j.orggeochem.2026.105189
Mostofian, B., Zhuang, T., Cheng, X., Nickels, J.D., 2019. Branched-Chain Fatty Acid Content Modulates Structure, Fluidity, and Phase in Model Microbial Cell Membranes. J. Phys. Chem. B 123, 5814–5821. https://doi.org/10.1021/acs.jpcb.9b04326

Oyaizu, H., Komagata, K., 1983. Grouping of Pseudomonas species on the basis of cellular fatty acid composition and the quinone system with special reference to the existence of 3-hydroxy fatty acids. J. Gen. Appl. Microbiol. 29, 17–40. https://doi.org/10.2323/jgam.29.17

PAGES 2k Consortium, 2013. Continental-scale temperature variability during the past two millennia. Nature Geosci 6, 339–346. https://doi.org/10.1038/ngeo1797

Pan, F., Yuan, H., Song, J., Yao, Q., Li, X., Duan, L., Xing, J., 2023. 3-Hydroxy fatty acids as proxies for seawater temperature and pH in the eastern China marginal seas. Chemical Geology 617, 121258. https://doi.org/10.1016/j.chemgeo.2022.121258

Pearson, E.J., Juggins, S., Allbrook, H., Foster, L.C., Hodgson, D.A., Naafs, B.D.A., Phillips, T., Roberts, S.J., 2025. Development of new global lake brGDGT-temperature calibrations: advances, applications, challenges, and recommendations. Quaternary Science Reviews 369, 109615. https://doi.org/10.1016/j.quascirev.2025.109615

Peter, H., Sommaruga, R., 2016. Shifts in diversity and function of lake bacterial communities upon glacier retreat. The ISME Journal 10, 1545–1554. https://doi.org/10.1038/ismej.2015.245

Poger, D., Caron, B., Mark, A.E., 2014. Effect of Methyl-Branched Fatty Acids on the Structure of Lipid Bilayers. J. Phys. Chem. B 118, 13838–13848. https://doi.org/10.1021/jp503910r

Pontes, D.S., Pinheiro, F.A., Lima-Bittencourt, C.I., Guedes, R.L.M., Cursino, L., Barbosa, F., Santos, F.R., Chartone-Souza, E., Nascimento, A.M.A., 2009. Multiple Antimicrobial Resistance of Gram-Negative Bacteria from Natural Oligotrophic Lakes Under Distinct Anthropogenic Influence in a Tropical Region. Microb Ecol 58, 762–772. https://doi.org/10.1007/s00248-009-9539-3

Raberg, J.H., Harning, D.J., Crump, S.E., De Wet, G., Blumm, A., Kopf, S., Geirsdóttir, Á., Miller, G.H., Sepúlveda, J., 2021. Revised fractional abundances and warm-season temperatures substantially improve brGDGT calibrations in lake sediments. Biogeosciences 18, 3579–3603. https://doi.org/10.5194/bg-18-3579-2021

Shang, Y., Wu, X., Wang, X., Wei, Q., Ma, S., Sun, G., Zhang, Huanxin, Wang, L., Dou, H., Zhang, Honghai, 2022. Factors affecting seasonal variation of microbial community structure in Hulun Lake, China. Science of The Total Environment 805, 150294. https://doi.org/10.1016/j.scitotenv.2021.150294

Sinninghe Damsté, J.S., Rijpstra, W.I.C., Foesel, B.U., Huber, K.J., Overmann, J., Nakagawa, S., Kim, J.J., Dunfield, P.F., Dedysh, S.N., Villanueva, L., 2018. An overview of the occurrence of ether- and ester-linked iso-diabolic acid membrane lipids in microbial cultures of the Acidobacteria: Implications for brGDGT paleoproxies for temperature and pH. Organic Geochemistry 124, 63–76. https://doi.org/10.1016/j.orggeochem.2018.07.006

Sinninghe Damsté, J.S., Rijpstra, W.I.C., Hopmans, E.C., Weijers, J.W.H., Foesel, B.U., Overmann, J., Dedysh, S.N., 2011. 13,16-Dimethyl Octacosanedioic Acid (iso -Diabolic Acid), a Common Membrane-Spanning Lipid of Acidobacteria Subdivisions 1 and 3. Appl Environ Microbiol 77, 4147–4154. https://doi.org/10.1128/AEM.00466-11

Stabili, L., Cavallo, R.A., 2004. Biodiversity of culturable heterotrophic bacteria in the Southern Adriatic Sea Italian coastal waters. Sci. mar. 68, 31–41. https://doi.org/10.3989/scimar.2004.68s131

Sun, Q., Chu, G., Liu, M., Xie, M., Li, S., Ling, Y., Wang, X., Shi, L., Jia, G., Lü, H., 2011. Distributions and temperature dependence of branched glycerol dialkyl glycerol tetraethers in recent lacustrine sediments from China and Nepal. J. Geophys. Res. 116, G01008. https://doi.org/10.1029/2010JG001365

Tebaldi, C., Ranasinghe, R., Vousdoukas, M., Rasmussen, D.J., Vega-Westhoff, B., Kirezci, E., Kopp, R.E., Sriver, R., Mentaschi, L., 2021. Extreme sea levels at different global warming levels. Nat. Clim. Chang. 11, 746–751. https://doi.org/10.1038/s41558-021-01127-1

Tierney, J.E., Russell, J.M., 2009. Distributions of branched GDGTs in a tropical lake system: Implications for lacustrine application of the MBT/CBT paleoproxy. Organic Geochemistry 40, 1032–1036. https://doi.org/10.1016/j.orggeochem.2009.04.014

Van Bree, L.G.J., Peterse, F., Baxter, A.J., De Crop, W., Van Grinsven, S., Villanueva, L., Verschuren, D., Sinninghe Damsté, J.S., 2020. Seasonal variability and sources of in situ brGDGT production in a permanently stratified African crater lake. Biogeosciences 17, 5443–5463. https://doi.org/10.5194/bg-17-5443-2020

Véquaud, P., Derenne, S., Thibault, A., Anquetil, C., Bonanomi, G., Collin, S., Contreras, S., Nottingham, A.T., Sabatier, P., Salinas, N., Scott, W.P., Werne, J.P., Huguet, A., 2021. Development of global temperature and pH calibrations based on bacterial 3-hydroxy fatty acids in soils. Biogeosciences 18, 3937–3959. https://doi.org/10.5194/bg-18-3937-2021

Wang, C., Bendle, J., Yang, Y., Yang, H., Sun, H., Huang, J., Xie, S., 2016. Impacts of pH and temperature on soil bacterial 3-hydroxy fatty acids: Development of novel terrestrial proxies. Organic Geochemistry 94, 21–31. https://doi.org/10.1016/j.orggeochem.2016.01.010

Wang, C., Bendle, J.A., Yang, H., Yang, Y., Hardman, A., Yamoah, A., Thorpe, A., Mandel, I., Greene, S.E., Huang, J., Xie, S., 2021. Global calibration of novel 3-hydroxy fatty acid based temperature and pH proxies. Geochimica et Cosmochimica Acta 302, 101–119. https://doi.org/10.1016/j.gca.2021.03.010

Wang, H., Yang, Y., Wang, C., Xie, S., 2025. Sources of bacterial 3-hydroxy fatty acids in Liangzihu Lake from central China: Implications for paleoclimate reconstruction. Organic Geochemistry 203, 104949. https://doi.org/10.1016/j.orggeochem.2025.104949

Watson, B.I., Williams, J.W., Russell, J.M., Jackson, S.T., Shane, L., Lowell, T.V., 2018. Temperature variations in the southern Great Lakes during the last deglaciation: Comparison between pollen and GDGT proxies. Quaternary Science Reviews 182, 78–92. https://doi.org/10.1016/j.quascirev.2017.12.011

Weber, Y., Sinninghe Damsté, J.S., Zopfi, J., De Jonge, C., Gilli, A., Schubert, C.J., Lepori, F., Lehmann, M.F., Niemann, H., 2018. Redox-dependent niche differentiation provides evidence for multiple bacterial sources of glycerol tetraether lipids in lakes. Proc. Natl. Acad. Sci. U.S.A. 115, 10926–10931. https://doi.org/10.1073/pnas.1805186115

Weijers, J.W.H., Bernhardt, B., Peterse, F., Werne, J.P., Dungait, J.A.J., Schouten, S., Sinninghe Damsté, J.S., 2011. Absence of seasonal patterns in MBT–CBT indices in mid-latitude soils. Geochimica et Cosmochimica Acta 75, 3179–3190. https://doi.org/10.1016/j.gca.2011.03.015

Weijers, J.W.H., Schouten, S., Van Den Donker, J.C., Hopmans, E.C., Sinninghe Damsté, J.S., 2007. Environmental controls on bacterial tetraether membrane lipid distribution in soils. Geochimica et Cosmochimica Acta 71, 703–713. https://doi.org/10.1016/j.gca.2006.10.003

Weise, L., Ulrich, A., Moreano, M., Gessler, A., E. Kayler, Z., Steger, K., Zeller, B., Rudolph, K., Knezevic-Jaric, J., Premke, K., 2016. Water level changes affect carbon turnover and microbial community composition in lake sediments. FEMS Microbiology Ecology 92, fiw035. https://doi.org/10.1093/femsec/fiw035

Wickham, H., 2009. stringr: Simple, Consistent Wrappers for Common String Operations. https://doi.org/10.32614/CRAN.package.stringr

Wu, J., Yang, H., Pancost, R.D., Naafs, B.D.A., Qian, S., Dang, X., Sun, H., Pei, H., Wang, R., Zhao, S., Xie, S., 2021. Variations in dissolved O2 in a Chinese lake drive changes in microbial communities and impact sedimentary GDGT distributions. Chemical Geology 579, 120348. https://doi.org/10.1016/j.chemgeo.2021.120348

Wu, J., Yang, H., Shen, C., Zhu, L., Pei, H., Dang, X., Huang, M., Xie, S., 2023. BrGDGT-based quantitative reconstructions of paleotemperature in lakes: Regional vs. site-specific calibrations. Quaternary Science Reviews 322, 108416. https://doi.org/10.1016/j.quascirev.2023.108416

Yang, Y., Wang, C., Bendle, J.A., Luo, Z., Dang, X., Xue, J., Xiang, X., Xie, S., 2021. Appraisal of paleoclimate indices based on bacterial 3-hydroxy fatty acids in 20 Chinese alkaline lakes. Organic Geochemistry 160, 104277. https://doi.org/10.1016/j.orggeochem.2021.104277

Yang, Y., Wang, C., Yan, Y., Sun, A., Yang, H., Xie, S., 2025. Distribution of bacterial 3-OH-FAs in Chinese saline lakes and its implication for paleoclimate reconstruction. Chemical Geology 677, 122630. https://doi.org/10.1016/j.chemgeo.2025.122630

Yannarell, A.C., Triplett, E.W., 2005. Geographic and Environmental Sources of Variation in Lake Bacterial Community Composition. Appl Environ Microbiol 71, 227–239. https://doi.org/10.1128/AEM.71.1.227-239.2005

Zeng, T., Chen, Y., Wu, R., Wang, H., Yang, Y., Yang, H., Huang, X., Luo, G., Wang, C., 2026. Deciphering the response of 3-hydroxy fatty acids to soil pH variation: influence of microbial community dynamics and membrane lipid remodelling. Geochimica et Cosmochimica Acta 417, 351–363. https://doi.org/10.1016/j.gca.2025.12.045

Zhang, Z., Li, J., Lu, H., Yang, H., Zhang, Y., Tang, Y., Fu, M., Peng, X., 2024. Bacterial glycerol tetraethers as a potential tool to trace marine methane cycling. Limnology & Oceanography 69, 104–120. https://doi.org/10.1002/lno.12462

Zhao, B., Castañeda, I.S., Bradley, R.S., Salacup, J.M., De Wet, G.A., Daniels, W.C., Schneider, T., 2021. Development of an in situ branched GDGT calibration in Lake 578, southern Greenland. Organic Geochemistry 152, 104168. https://doi.org/10.1016/j.orggeochem.2020.104168

Zhou, J., Kang, D., Chen, S., Dong, L., 2026. Machine learning-based paleobathymetric reconstructions using archaeal lipid biomarkers. Science Advances 12, 8. https://doi.org/10.1126/sciadv.adz3284

Zhu, Z., Wu, J., Chu, G., Liu, J., 2025. New global lacustrine brGDGTs temperature calibrations based on machine learning. Quaternary Science Reviews 357, 109319. https://doi.org/10.1016/j.quascirev.2025.109319

Zhu, Z., Wu, J., Rioual, P., Mingram, J., Yang, H., Zhang, B., Chu, G., Liu, J., 2021. Evaluation of the sources and seasonal production of brGDGTs in lake Sihailongwan (N.E. China) and application to reconstruct paleo-temperatures over the period 60–8 ka BP. Quaternary Science Reviews 261, 106946. https://doi.org/10.1016/j.quascirev.2021.106946

Figure Captions

Figure 1. Location of the surface lacustrine sediments for which the distribution of 3-OH FAs was investigated. The surface sediments analyzed in this study (*n*=128) are presented in blue. The surface sediments previously studied by Hou et al. (2026; *n*=21) are presented in green, those by Ke et al. (2026; *n*=72) in yellow) and those by Yang et al. (2021; *n*=20) in red.

Figure 2. Distribution of MAAT (°C), MAF (°C), MST (°C), MAP (mm), and elevation (m) for the global 3-OH FA lacustrine dataset, comprising samples from this study (*n*=128), Hou et al. (2026; *n*=21), Ke et al. (2026; *n*=72), and Yang et al. (2021; *n*=20).

Figure 3. Mean relative abundance of 3-OH FAs in lakes (*n*=241; this study; Ke et al., 2026; Yang et al., 2021; Hou et al., 2026), soils (*n*=309; Huguet et al., 2019; Véquaud et al., 2021; Wang et al., 2016&2021), and oceans (*n*=41; Pan et al., 2023).

Figure 4. PCA of all 3-OH FA data available so far in lakes (*n*=241; this study; Ke et al., 2026; Yang et al., 2021; Hou et al., 2026), soils (*n*=309; Huguet et al., 2019; Véquaud et al., 2021; Wang et al., 2016 and 2021), and oceans (*n*=41; Pan et al., 2023).

Figure 5. Distributions of temperature, elevation, precipitation, and pH in the 3 clusters. The pH data are available for 120 lakes. The violin shape plot shows the normalized distribution of the factors, while the mean value is shown as a horizontal bar inside the box plot on top. The box represents the middle 50% of the observations.

Figure 6. Geographical distribution of the global lake samples related to the three 3-OH FA clusters (*n*=241; this study; Ke et al., 2026; Yang et al., 2021; Hou et al., 2026).

Figure 7. PCA of 3-OH FAs in lakes (*n*=241; this study; Ke et al., 2026; Yang et al., 2021; Hou et al., 2026). Three clusters were defined by hierarchical clustering: Cluster 1 (*n*=67), Cluster 2 (*n*=105), and Cluster 3 (*n*=69).

Figure 8. Correlation matrix of the 3-OH FA relative abundances and associated indices in the global lake dataset (*n*=241; this study; Ke et al., 2026; Yang et al., 2021; Hou et al., 2026) with the mean annual air temperature (MAAT), average temperature of months above freezing (MAF), and mean summer temperature (MST). Significant correlations ($p<0.05$) are labelled with *.

Figure 9. Modelled temperature (MAAT, MAF and MST) predictions *versus* observed values, and associated residuals. All the models made predictions that were 10-fold cross-validated. The predictions of the TabPFN and Multilinear models are based on the full profile of the 3-OH FAs in global lakes (*n*=241), whereas the RF models are based on the 15 variables with the highest relative importance. Outliers were excluded following Rosner analyses for the three models: TabPFN (*n*=6; 6; 3 for MAAT, MAF and MST respectively), RF (*n*=1; 4; 2 for MAAT, MAF and MST respectively), and multilinear (*n*=3; 3; 1 for MAAT, MAF and MST respectively).

Figure 10. Relative importance of the individual 3-OH FAs in the RF models with MAAT (left), MAF (middle) and MST (right) based on the permutation importance method (Breiman, 2001). These models were built using the global lake 3-OH FA dataset (*n*=241).

Figure 11. Reconstruction of temperatures over the last 2000 years in Lake Blauvelt based on 3-OH FA and brGDGT data presented in Hou et al. (2026). The horizontal dashed line

represents the modern temperature at this site and is also labelled in red. The light blue panel spans the Little Ice Age (LIA) period (between 1550 to 1850 Yr cal CE). **Panels a, c, e**: temperatures reconstructed using the global 3-OH FA TabPFN, Random Forest (RF), and multilinear regression models proposed in the present study for global lacustrine dataset (*n*=249). MAAT, MAF and MST are presented in panels a, c, and e, respectively. Additionally, in panel c, MAF reconstructed from global temperature models based on MBT'$_{5Me}$ are also presnted (calibration 1 from Zhu et al., 2025; Martínez-Sosa et al., 2021). **Panels b, d and f**: temperatures reconstructed using regional 3-OH FA TabPFN and Random Forest (RF) models trained with 21 lakes of the East Coast U.S. The temperature estimates obtained from regional RAN$_{13}$ and MBT'$_{5Me}$ calibrations (Hou et al., 2026) are provided for comparison. MAAT, MAF and MST are presented in panels b, d, and f, respectively.

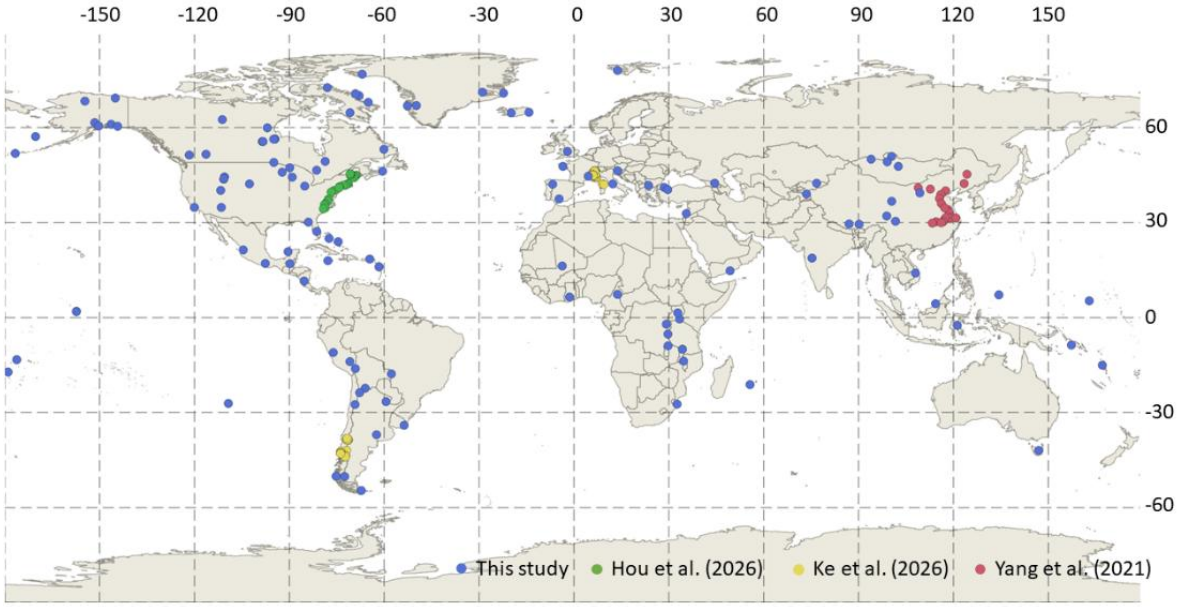
-150
-120
-90
-60
-30
0
30
60
90
120
150
60
30
0
-30
-60
This study
Hou et al. (2026)
Ke et al. (2026)
Yang et al. (2021)

Figure 1

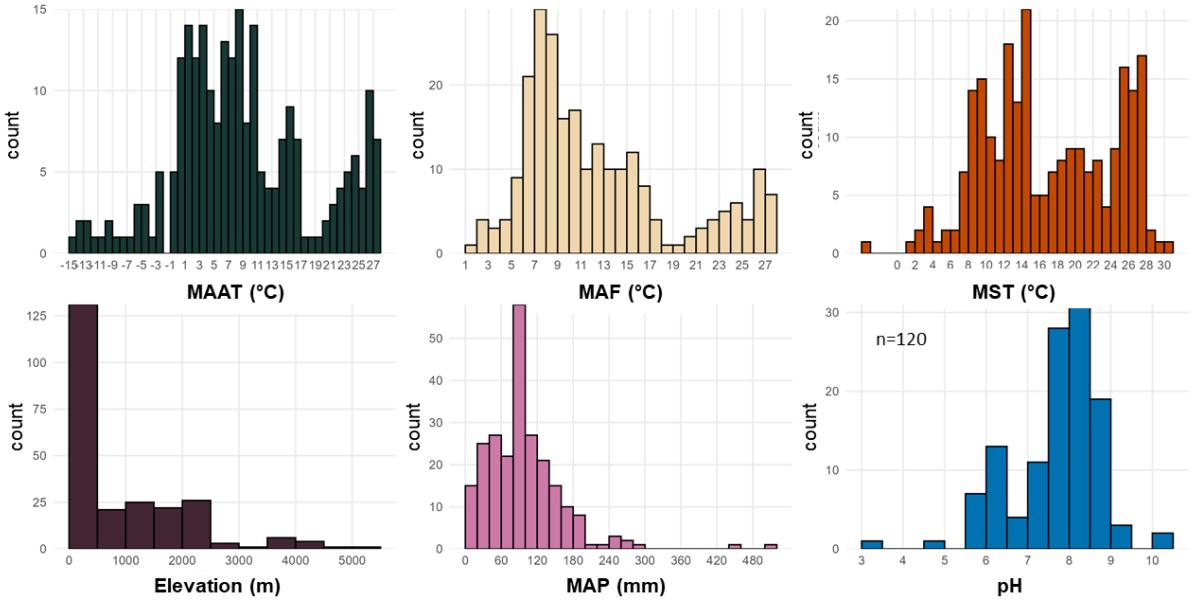

Figure 2

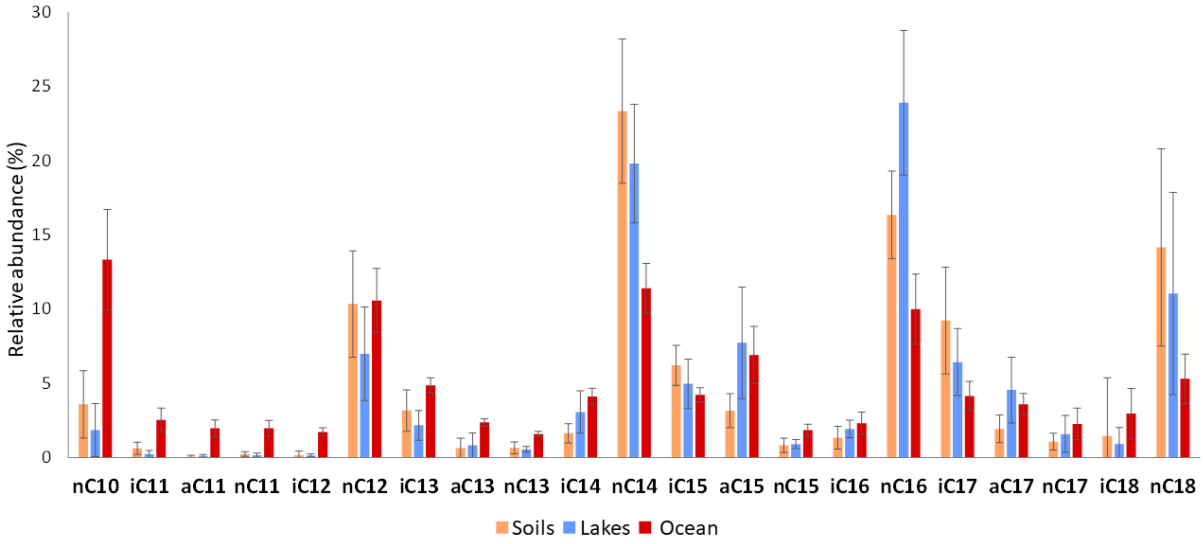
30
25
20
15
10
5
0
Relative abundance (%)
nC10
iC11
aC11
nC11
iC12
nC12
iC13
aC13
nC13
iC14
nC14
iC15
aC15
nC15
iC16
nC16
iC17
aC17
nC17
iC18
nC18
Soils
Lakes
Ocean

Figure 3

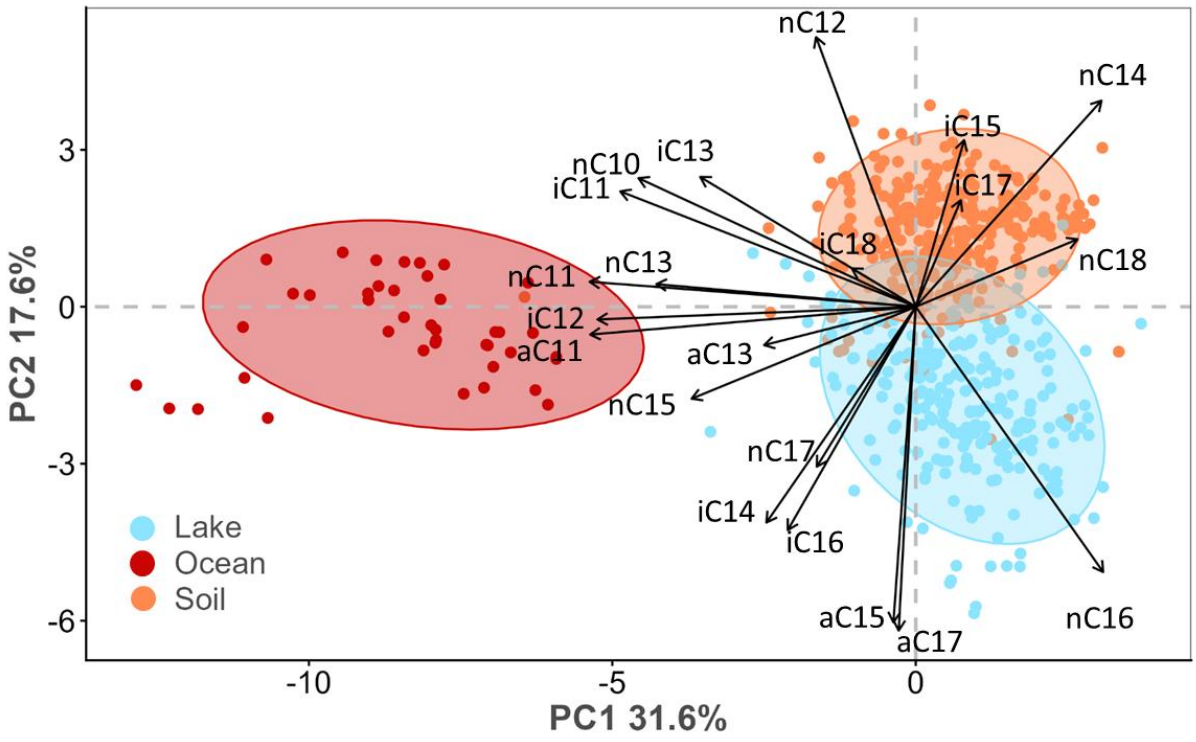
nC12
nC14
iC15
iC13
nC10
iC11
iC17
iC18
nC18
nC13
nC11
iC12
aC11
aC13
nC15
nC17
iC14
iC16
aC15
aC17
nC16
Lake
Ocean
Soil
PC2 17.6%
PC1 31.6%
3
0
-3
-6
-10
-5
0

Figure 4

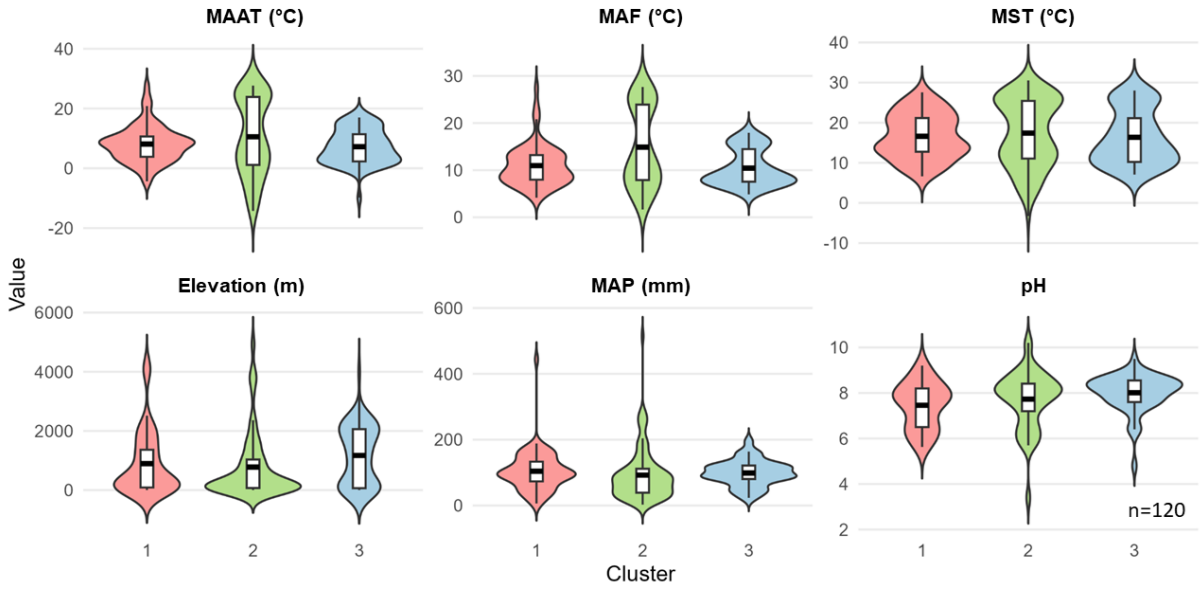

Figure 5

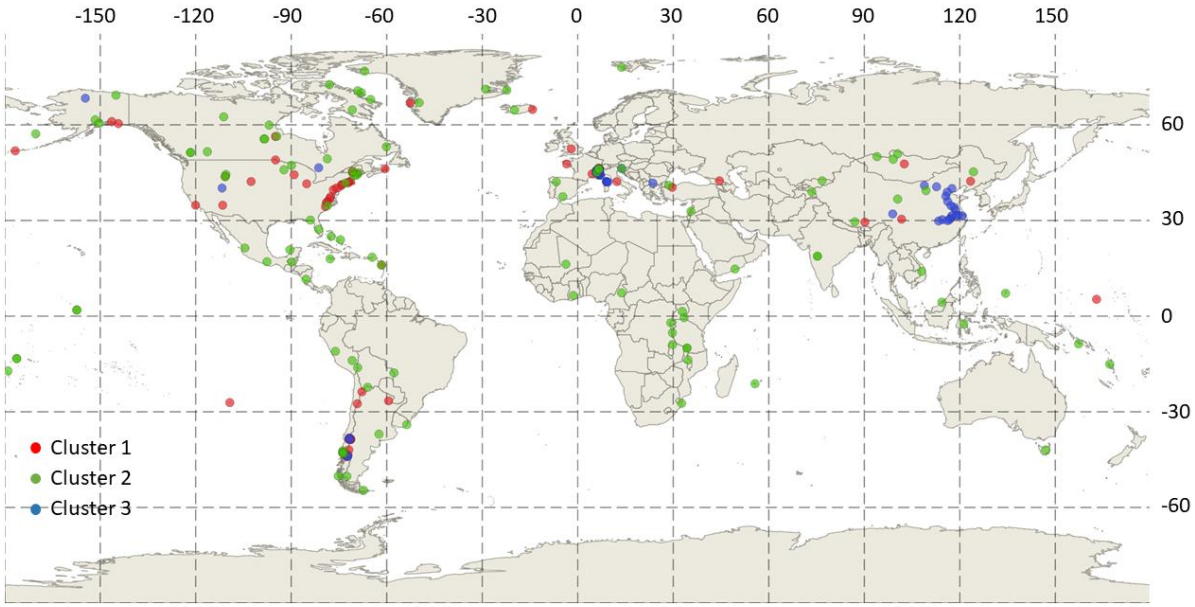
-150
-120
-90
-60
-30
0
30
60
90
120
150
60
30
0
-30
-60
Cluster 1
Cluster 2
Cluster 3

Figure 6

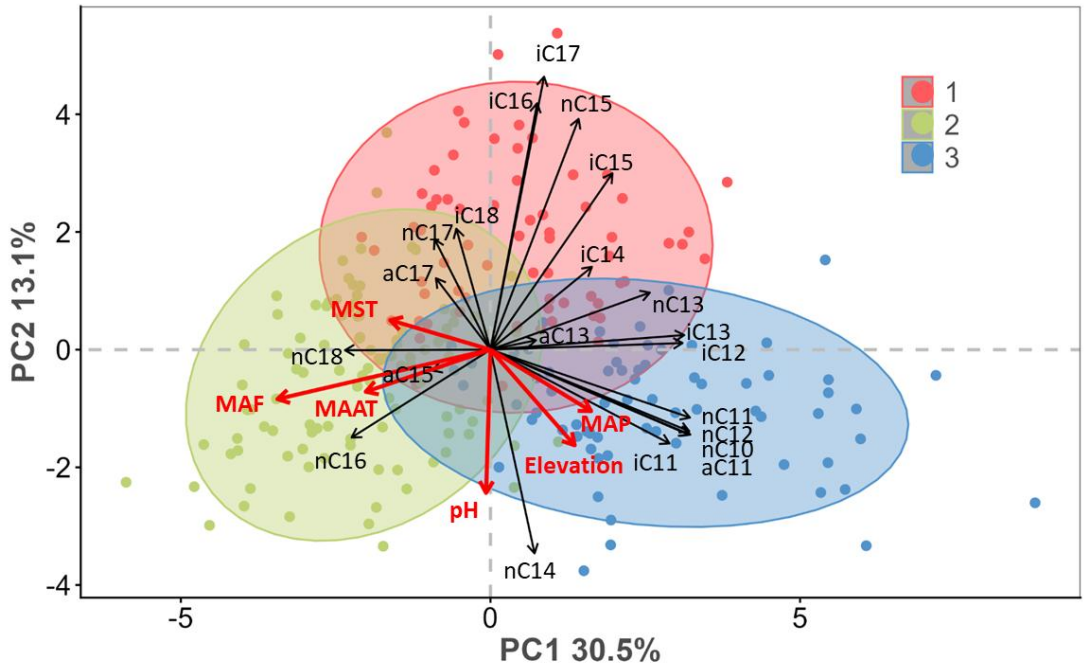
iC17
iC16
nC15
iC15
iC18
nC17
iC14
aC17
nC13
MST
aC13
iC13
iC12
nC18
aC15
MAF
MAAT
MAP
nC11
nC12
nC10
aC11
nC16
Elevation
iC11
pH
nC14
1
2
3
PC2 13.1%
PC1 30.5%
4
2
0
-2
-4
-5
0
5

Figure 7

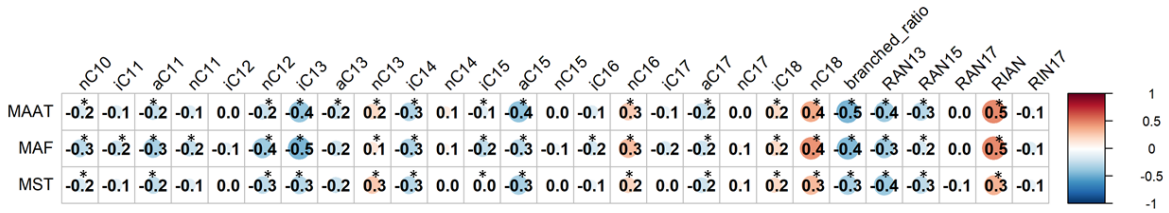
nC10
iC11
aC11
nC11
iC12
nC12
iC13
aC13
nC13
iC14
nC14
iC15
aC15
nC15
iC16
nC16
iC17
aC17
nC17
iC18
nC18
branched_ratio
RAN13
RAN15
RAN17
RIAN
RIN17
MAAT -0.2 -0.1 -0.2 -0.1 0.0 -0.2 -0.4 -0.2 0.2 -0.3 0.1 -0.1 -0.4 0.0 -0.1 0.3 -0.1 -0.2 0.0 0.2 0.4 -0.5 -0.4 -0.3 0.0 0.5 -0.1
MAF -0.3 -0.2 -0.3 -0.2 -0.1 -0.4 -0.5 -0.2 0.1 -0.3 0.1 -0.2 -0.3 -0.1 -0.2 0.3 -0.2 -0.2 0.1 0.2 0.4 -0.4 -0.3 -0.2 0.0 0.5 -0.1
MST -0.2 -0.1 -0.2 -0.1 0.0 -0.3 -0.3 -0.2 0.3 -0.3 0.0 0.0 -0.3 0.0 -0.1 0.2 0.0 -0.2 0.1 0.2 0.3 -0.3 -0.4 -0.3 -0.1 0.3 -0.1
1
0.5
0
-0.5
-1

Figure 8

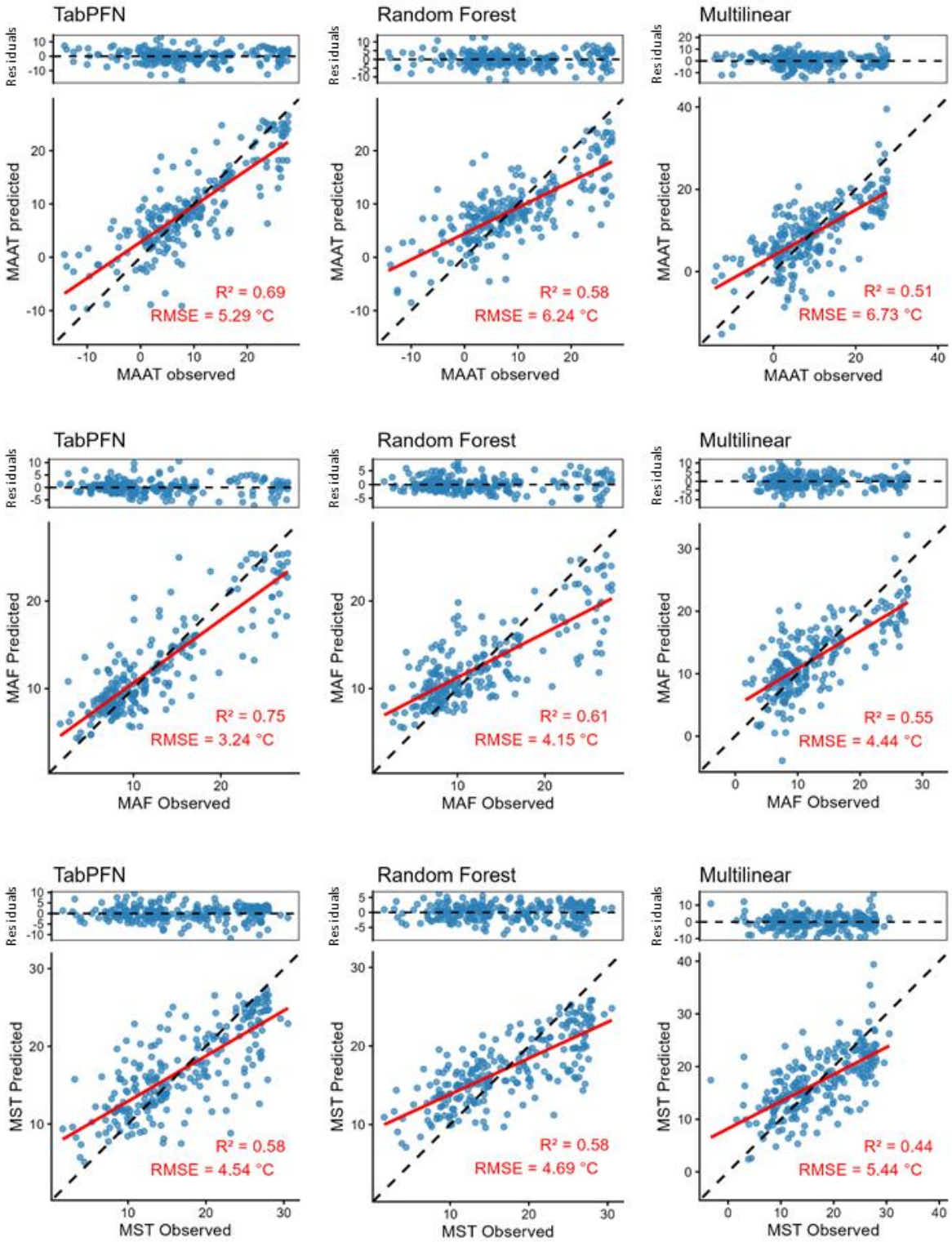
TabPFN
Random Forest
Multilinear
Residuals
MAAT predicted
MAAT observed
R² = 0.69
RMSE = 5.29 °C
R² = 0.58
RMSE = 6.24 °C
R² = 0.51
RMSE = 6.73 °C
MAF Predicted
MAF Observed
R² = 0.75
RMSE = 3.24 °C
R² = 0.61
RMSE = 4.15 °C
R² = 0.55
RMSE = 4.44 °C
MST Predicted
MST Observed
R² = 0.58
RMSE = 4.54 °C
R² = 0.58
RMSE = 4.69 °C
R² = 0.44
RMSE = 5.44 °C

Figure 9

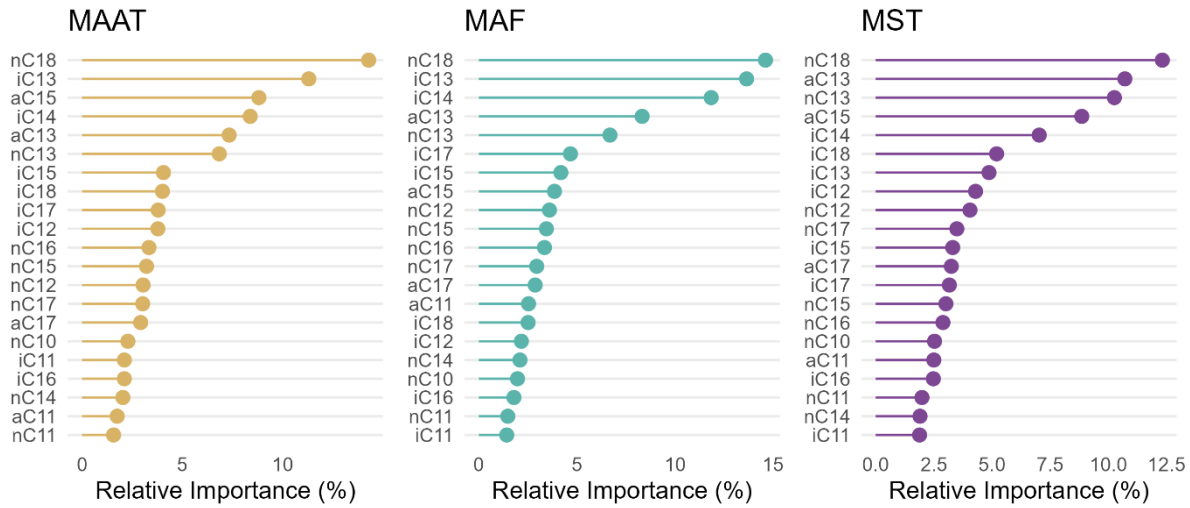
MAAT
nC18
iC13
aC15
iC14
aC13
nC13
iC15
iC18
iC17
iC12
nC16
nC15
nC12
nC17
aC17
nC10
iC11
iC16
nC14
aC11
nC11
0
5
10
Relative Importance (%)
MAF
nC18
iC13
iC14
aC13
nC13
iC17
iC15
aC15
nC12
nC15
nC16
nC17
aC17
aC11
iC18
iC12
nC14
nC10
iC16
nC11
iC11
0
5
10
15
Relative Importance (%)
MST
nC18
aC13
nC13
aC15
iC14
iC18
iC13
iC12
nC12
nC17
iC15
aC17
iC17
nC15
nC16
nC10
aC11
iC16
nC11
nC14
iC11
0.0
2.5
5.0
7.5
10.0
12.5
Relative Importance (%)

Figure 10

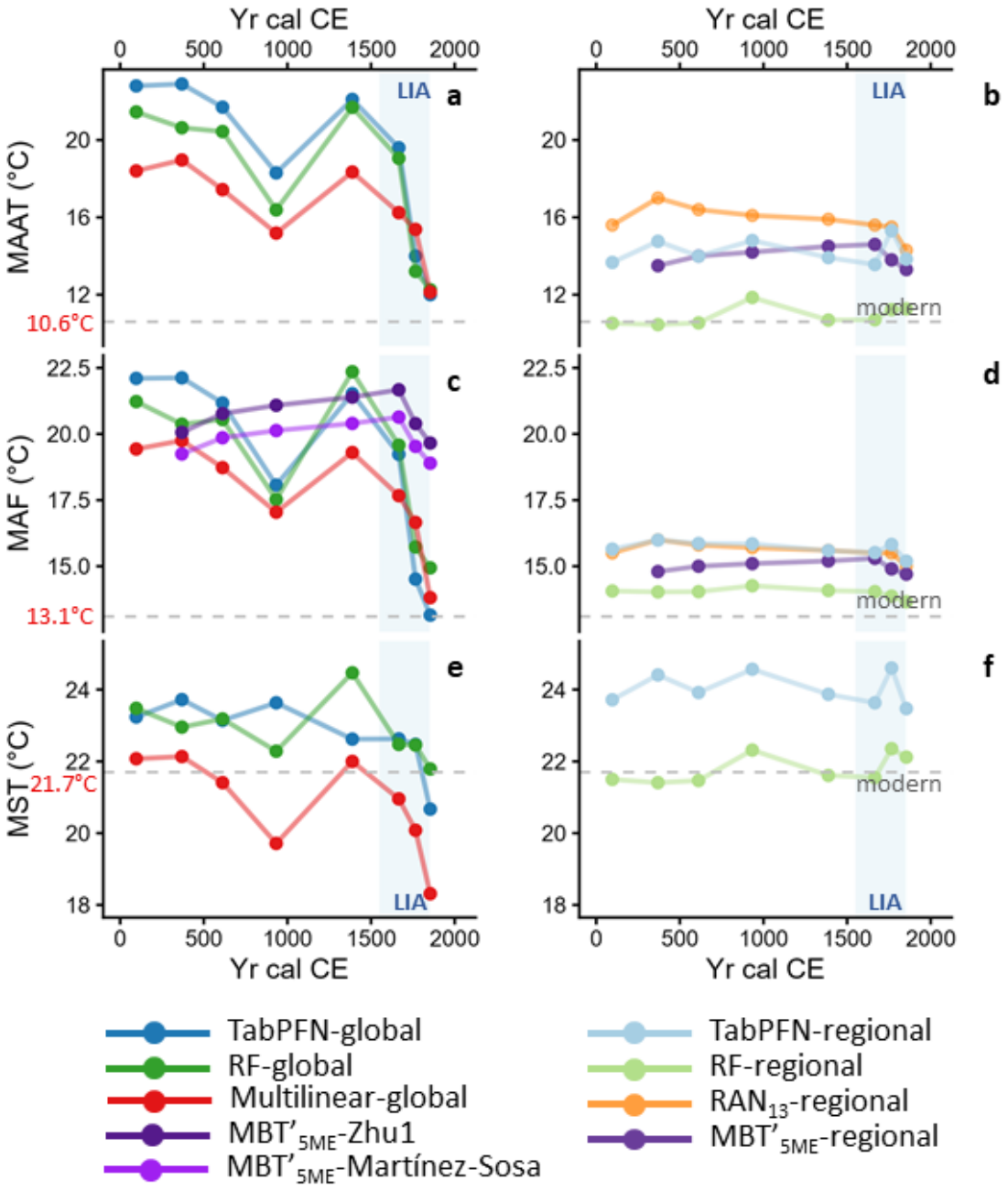
Yr cal CE
0
500
1000
1500
2000
LIA
a
b
c
d
e
f
MAAT (°C)
MAF (°C)
MST (°C)
10.6°C
13.1°C
21.7°C
modern
TabPFN-global
RF-global
Multilinear-global
MBT'5ME-Zhu1
MBT'5ME-Martínez-Sosa
TabPFN-regional
RF-regional
RAN13-regional
MBT'5ME-regional

Figure 11

Table S1. Outliers in the TabPFN model prediction identified by Rosner analysis. Lakes 1 to 5 are outliers in the MAAT prediction, whereas in the MAF prediction, an additional outlier (Lake 6) is observed.

	ID	Lake	Country	Latitude	Longitude
1	QLR-CHAL11	Challpa chocha	Peru	-13.91555	-70.86562
2	GREEN-BONE10	Bone Lake	Greenland	70.88778	-22.26664
3	LTS-RKU17	Rano Rakaku	Chile (Easter Island)	-27.12206	-109.29031
4	M93-MAL93	Lake Malawi	Mozambique	-10.00265	34.318217
5	SPCZ14-NIVA	Dranoniveilomo	Fiji	-17.197917	-178.956017
6	G16-GVA16	Lagoa Gaiva	Bolivia	-17.79217	-57.71796

Table S2. Lakes overlapping with the soil cluster in PCA that compares 3-OH FAs of lakes, soils, and ocean.

Lake	Cluster	Location	MAAT (°C)	MAF (°C)	MST (°C)	Reference
Conguillio	Cluster 1	Chile	7.4	7.9	13.4	Ke et al. (2026)
Laguna Negra	Cluster 1	Chile	8.8	10.2	14.6	Ke et al. (2026)
Lake Zhenzhu	Cluster 1	China	8.3	15.0	22.7	Yang et al. (2021)
CANAL-DUD14	Cluster 1	UK	9.1	9.1	14.8	This study
Lake Chagan	Cluster 2	China	4.9	15.6	22.0	Yang et al. (2021)
EAU20-01 W	Cluster 2	Réunion	13.0	13.0	15.8	This study
JUDD-JD11	Cluster 2	US (Alaska)	0.4	9.9	12.3	This study
JOSE19-5X	Cluster 2	Chile	6.6	6.6	9.4	This study
Cajunco	Cluster 2	Chile	10.8	10.3	13.4	Ke et al. (2026)
Cipreses	Cluster 2	Chile	10.8	10.7	14.0	Ke et al. (2026)
Renihue	Cluster 2	Chile	10.4	9.6	12.9	Ke et al. (2026)
Jones Lake	Cluster 2	US	16.5	16.5	25.4	Hou et al. (2026)
BPP-MDM11	Cluster 2	Brunei Darussalam	27.1	27.1	27.3	This study
Nino	Cluster 3	French Alps	6.8	8.1	14.3	Ke et al. (2026)
Verde Conguillio	Cluster 3	Chile	8.2	8.8	14.3	Ke et al. (2026)
Noir	Cluster 3	French Alps	4.0	7.7	12.3	Ke et al. (2026)
Claro del solar	Cluster 3	Chile	8.0	10.1	14.8	Ke et al. (2026)
Lauvitel	Cluster 3	French Alps	5.1	7.6	13.2	Ke et al. (2026)
Vianney	Cluster 3	French Alps	1.0	6.3	8.7	Ke et al. (2026)
Vallons	Cluster 3	French Alps	4.3	8.9	14.2	Ke et al. (2026)
Domenon	Cluster 3	French Alps	0.7	6.0	8.4	Ke et al. (2026)
Baiyangdian	Cluster 3	China	12.2	15.8	25.8	Yang et al. (2021)
Laouchet	Cluster 3	French Alps	1.1	6.3	8.5	Ke et al. (2026)
VBL-COATA07	Cluster 3	Bulgaria	6.5	9.4	14.9	This study
Tantauco	Cluster 3	Chile	10.2	9.3	12.7	Ke et al. (2026)
Melo	Cluster 3	French Alps	6.5	7.4	13.6	Ke et al. (2026)

Table S3. Temperature reconstructions of the sediment core of Lake Blauvelt, USA.

		MAAT(°C)							
				TabPFN		RF		ML	
Sample	Age (BP)	RAN_{13}	MBT'_{5ME}	Regional	Global	Regional	Global	Regional	Global
LB-16	96	14.3	13.3	13.8	12.0	11.3	12.3	133.8	12.1
LB-26	184	15.5	13.8	15.3	14.0	11.2	13.2	167.6	15.4
LB-36	284	15.6	14.6	13.6	19.6	10.7	19.1	275.8	16.2
LB-46	562	15.9	14.5	13.9	22.1	10.7	21.7	153.3	18.3
LB-66	1017	16.1	14.2	14.8	18.3	11.9	16.4	46.9	15.2
LB-76	1338	16.4	14.0	14.0	21.7	10.5	20.4	352.3	17.4
LB-85	1581	17.0	13.5	14.8	22.9	10.5	20.6	231.4	19.0
LB-93	1854	15.6		13.7	22.8	10.5	21.5	247.6	18.4

		MAF (°C)							
				TabPFN		RF		ML	
Sample	Age (BP)	RAN_{13}	MBT'_{5ME}	Regional	Global	Regional	Global	Regional	Global
LB-16	96	15.0	14.7	15.2	13.2	13.7	14.9	53.5	13.8
LB-26	184	15.5	14.9	15.8	14.5	13.9	15.7	64.8	16.7
LB-36	284	15.5	15.3	15.5	19.2	14.0	19.6	93.8	17.7
LB-46	562	15.6	15.2	15.6	21.5	14.1	22.4	51.5	19.3
LB-66	1017	15.7	15.1	15.8	18.1	14.3	17.5	14.1	17.0
LB-76	1338	15.8	15.0	15.9	21.2	14.0	20.5	117.7	18.7
LB-85	1581	16.0	14.8	16.0	22.1	14.0	20.4	77.8	19.8
LB-93	1854	15.5		15.6	22.1	14.1	21.2	80.1	19.4

		MST(°C)					
		TabPFN		RF		ML	
Sample	Age (BP)	Regional	Global	Regional	Global	Regional	Global
LB-16	96	23.5	20.7	22.1	21.8	76.4	18.3
LB-26	184	24.6	22.5	22.4	22.5	94.1	20.1
LB-36	284	23.6	22.6	21.5	22.5	137.9	21.0
LB-46	562	23.9	22.6	21.6	24.5	90.9	22.0
LB-66	1017	24.6	23.6	22.3	22.3	47.7	19.7
LB-76	1338	23.9	23.1	21.5	23.2	169.7	21.4
LB-85	1581	24.4	23.7	21.4	23.0	122.9	22.1
LB-93	1854	23.7	23.2	21.5	23.5	129.8	22.1